J. Fluid Mech. (2020), *vol.* 883, A56. © Cambridge University Press 2019
doi:10.1017/jfm.2019.825

Quasi-local method of wave decomposition in a slowly varying medium

Yohei Onuki†

Research Institute for Applied Mechanics, Kyushu University, 6-1 Kasuga-koen, Kasuga, Fukuoka, Japan

(Received 6 December 2018; revised 4 August 2019; accepted 8 October 2019)

The general asymptotic theory for wave propagation in a slowly varying medium, classically known as the Wentzel–Kramers–Brillouin–Jeffreys (WKBJ) approximation, is revisited here with the aim of constructing a new data diagnostic technique useful in atmospheric and oceanic sciences. Using the Wigner transform, a kind of mapping that associates a linear operator with a function, we analytically decompose a flow field into mutually independent wave signals. This method takes account of the variations in the polarisation relations, an eigenvector that represents the kinematic characteristics of each wave component, so as to project the variables onto their eigenspace quasi-locally. The temporal evolution of a specific mode signal obeys a single wave equation characterised by the dispersion relation that also incorporates the effect from the local gradient in the medium. Combining this method with transport theory and applying them to numerical simulation data, we can detect the transfer of energy or other conserved quantities associated with the propagation of each wave signal in a wide variety of situations.

Key words: waves in rotating fluids, computational methods

1. Introduction

Various physical processes arising in a rotating stratified fluid are largely explained in terms of wave dynamics. Waves generated by external, or sometimes internal, forcing propagate spatially in a fluid, transporting momentum and energy, which are fundamental ingredients of the large-scale steady motions in the atmosphere (Yiğit & Medvedev 2015) and the ocean (MacKinnon *et al.* 2017). Over the last couple of decades, owing to the development of computational power, more and more accurate numerical simulation systems have been developed to reproduce the interaction between the mean state and fluctuating waves in the atmosphere and ocean. Accordingly, extraction of wave signals from the model output data that involve physical variables such as velocity, density and pressure, and evaluation of their impacts on the larger-scale flow field have become increasingly important tasks. For this purpose, advanced diagnostic tools have been invented to illustrate the geography of the wave properties, such as energy, momentum and their fluxes.

A series of studies, such as those of Plumb (1985), Takaya & Nakamura (1997), Takaya & Nakamura (2001), Kinoshita, Tomikawa & Sato (2010) and Kinoshita &

† Email address for correspondence: onuki@riam.kyushu-u.ac.jp

https://doi.org/10.1017/jfm.2019.825 Published online by Cambridge University Press

Sato (2013), provide examples in which the pseudo-momentum flux associated with Rossby waves (RWs) and inertia–gravity waves (IGWs) is formulated so as to be calculable using data obtained from general atmospheric models. An assumption underlying these methods is that spatial variation in the medium is much slower than the wave oscillation, so that all of the variables can be locally decomposable into plane monochromatic components, which are solutions of linear equations with constant coefficients. This scale separation assumption is frequently referred to as the Wentzel–Kramers–Brillouin–Jeffreys (WKBJ) approximation. The original WKBJ theory is, however, merely a solution method for differential equations (Bender & Orszag 1999). For data diagnostic purposes, instead of a solution, deriving a conservation equation in the form of

$$\frac{\partial A}{\partial t} + \boldsymbol{\nabla} \cdot \boldsymbol{F} = S, \tag{1.1}$$

and numerically computing $\boldsymbol{F}$ are the central objectives (see, e.g. Takaya & Nakamura 2001). Here A, $\boldsymbol{F}$ and S are the energy or pseudo-momentum density, its flux and the source or sink term, respectively. In the limit of a monochromatic wave train, $\boldsymbol{F}$ should be reduced to the product of A and the group velocity. To ensure this property is sometimes a difficult task (Aiki, Greatbatch & Claus 2017).

The background underlying this flux analysis is the transport theory (Ryzhik, Papanicolaou & Keller 1996; Guo & Wang 1999, and references therein). In this theory, the density of some conserved quantity is defined in physical and wavenumber space and its transfer is described by the transport equation,

$$\frac{\partial w}{\partial t} + \boldsymbol{\nabla}_x \cdot (w \boldsymbol{\nabla}_k \omega) - \boldsymbol{\nabla}_k \cdot (w \boldsymbol{\nabla}_x \omega) = s, \tag{1.2}$$

where $w(\boldsymbol{x}, \boldsymbol{k}, t)$ is the density of a conserved quantity, $\omega(\boldsymbol{x}, \boldsymbol{k})$ is the dispersion relation, $\boldsymbol{\nabla}_x$ and $\boldsymbol{\nabla}_k$ are gradients in physical and wavenumber space, respectively, and s represents source, decay and scattering effect. In this theory, wavenumber $\boldsymbol{k}$ is defined in a quasi-local sense: $(\boldsymbol{x}, \boldsymbol{k})$ specifies a wave packet with a local wavenumber $\boldsymbol{k}$ located in the vicinity of $\boldsymbol{x}$. The characteristics of (1.2) are specified by a set of equations, $\dot{\boldsymbol{x}} = \boldsymbol{\nabla}_k \omega$ and $\dot{\boldsymbol{k}} = -\boldsymbol{\nabla}_x \omega$, which represents the wave trajectory in physical and wavenumber space, and solving these equations is referred to as ray tracing (Lighthill 1978). When (1.2) is integrated in wavenumber space, the usual conservation equation (1.1) is derived.

The transport equation (1.2) is operationally used to predict the ocean surface state in the numerical models developed, such as that by WAMDI Group (1988). As for geophysical fluid dynamics, transport theory has been developed by Powell & Vanneste (2005), Wordsworth (2009), Danioux & Vanneste (2016), Savva & Vanneste (2018) and Kafiabad, Savva & Vanneste (2019). In recent years, the transport equation (1.2) has also been incorporated into the prediction systems for the ocean interior (Olbers & Eden 2013; Eden & Olbers 2017).

The aim of the current study is, however, neither to investigate a specific process using the transport theory nor to develop a numerical method to integrate the transport equation. Instead, the transport theory is here utilised for data diagnostic purposes. More specifically, this paper explores the method to compute the terms in the transport equation (1.2) using data produced from a common numerical model. A challenge in this work is to decompose different modes in a spatially varying medium.

https://doi.org/10.1017/jfm.2019.825 Published online by Cambridge University Press

In a rotating stratified fluid with the Boussinesq approximation, an arbitrary infinitesimal motion is regarded as a superposition of rapidly oscillating IGWs, sometimes called the wave mode, and the quasi-stationary vortical mode. If the coefficient parameters of the equations of motion, such as the Brunt–Väisälä frequency, the Coriolis parameter and the background mean velocity, are spatially constant, the two distinct modes can be clearly decomposed by taking the Fourier transform and projecting the variables onto the eigenvectors of the coefficient matrix of the equations. This eigenvector is called the polarisation relation and specifies the kinematic characteristics of each mode: the oscillation angle or the relative phases and amplitudes of the variables. The homogeneous wave–vortex decomposition technique has been frequently used to analyse flow field data (e.g. Lien & Müller 1992; Bühler, Callies & Ferrari 2014; Bühler, Kuang & Tabak 2017). If the system is inhomogeneous due to variations in coefficient parameters, the polarisation relations of both the wave and vortical modes vary from place to place so that the usual Fourier analysis becomes ineffective.

The difficulty is not only in the variations in the polarisation relations. The local dispersion relation of each mode is also modified due to the effect of gradients in parameters. For example, the gradient in the background potential vorticity due to the planetary β-effect (β represents the meridional variation in the Coriolis parameter) or topographic slope causes the vortical modes to oscillate as RWs. The gradient in the background flow velocity modifies the dispersion relation of IGWs, which substantially affects the propagation of near-inertial waves in a frontal area (Kunze 1985). The frequency shift due to inhomogeneity is explained by the WKBJ method when the higher-order terms in the phase of variables, which are called geometric phase, are analysed. In geophysical fluid dynamics, this phase shift has been considered for example by Bretherton (1968) and Vanneste & Shepherd (1999), and even made explicit by McKee (1973), but is commonly ignored in ray-tracing methods (Bühler 2014). Although Guo & Wang (1999) and Powell & Vanneste (2005) formulated a procedure to separately derive the transport equation for each mode in an inhomogeneous medium, their methods are still insufficient to incorporate the effect of the frequency shift.

To overcome the problems raised above, this study develops theoretical and numerical methods of wave decomposition properly taking account of the inhomogeneity of the system. The plan of this paper is as follows. In § 2, we discuss a general description of wave motions in an inviscid fluid system in terms of Wigner transform, which enables a set of simultaneous wave equations to be asymptotically decomposed into the ones governing mutually independent modes. Defining the Wigner distribution function, we subsequently derive the transport equation. In § 3, we take an example of a rotating shallow water model, in which variations in the Coriolis parameter and the depth cause slow propagation of the vortical mode as RWs. We confirm that the present method appropriately derives the dispersion relation of the RWs in a perturbation term, and therefore their propagation is well described in this framework. A simple numerical experiment is also conducted, which demonstrates the usefulness of this method for the diagnosis of model data. Discussion and conclusions are presented in § 4.

2. General description of wave decomposition and transport theory

2.1. *Linear waves in a non-canonical Hamiltonian system*

Since the purpose of this study is to offer a methodology of wave decomposition applicable to a wide variety of fluid systems, we begin with a mathematical

https://doi.org/10.1017/jfm.2019.825 Published online by Cambridge University Press

description of fluid motion in its most general form. According to Morrison (1998), evolution equations for an inviscid fluid are written in a non-canonical Hamiltonian form,

$$\frac{\partial \boldsymbol{v}}{\partial t} = \hat{\boldsymbol{J}}(\boldsymbol{v})\frac{\delta \mathcal{H}}{\delta \boldsymbol{v}}, \tag{2.1}$$

where the state vector $\boldsymbol{v}(\boldsymbol{x}, t) : \mathbb{R}^{d+1} \to \mathbb{R}^n$ represents physical variables such as velocity or spatial displacement of the medium, $\hat{\boldsymbol{J}}(\boldsymbol{v})$ is a nonlinear skew-Hermitian operator and $\mathcal{H}[\boldsymbol{v}]$ is a Hamiltonian functional generally consisting of the energy and some Casimir invariants. Assuming an infinitesimal fluctuation from a local minimum point of $\mathcal{H}$, which we write $\boldsymbol{v} = \boldsymbol{\Upsilon} + \boldsymbol{v}'$, the governing equation (2.1) becomes

$$\frac{\partial \boldsymbol{v}'}{\partial t} = \hat{\boldsymbol{J}}(\boldsymbol{\Upsilon})\left.\frac{\delta^2 \mathcal{H}}{\delta \boldsymbol{v}^2}\right|_{\boldsymbol{\Upsilon}} \boldsymbol{v}'. \tag{2.2}$$

Then, extending the definition of state vectors from real to complex variables and defining linear Hermitian operators, $\delta^2\mathcal{H}/\delta \boldsymbol{v}^2|_{\boldsymbol{\Upsilon}} \equiv \hat{\boldsymbol{A}}$ and $\mathrm{i}\hat{\boldsymbol{A}}\hat{\boldsymbol{J}}(\boldsymbol{\Upsilon})\hat{\boldsymbol{A}} \equiv \hat{\boldsymbol{B}}$, we rewrite (2.2) as

$$\mathrm{i}\hat{\boldsymbol{A}}\frac{\partial \boldsymbol{v}'}{\partial t} = \hat{\boldsymbol{B}}\boldsymbol{v}'. \tag{2.3}$$

In the following, † denotes the complex conjugate. According to (2.3), the functional $\mathcal{E}[\boldsymbol{v}'] \equiv (1/2)\int \boldsymbol{v}'^\dagger \hat{\boldsymbol{A}}\boldsymbol{v}' \mathrm{d}\boldsymbol{x}$ remains unchanged with time: $\mathrm{d}\mathcal{E}/\mathrm{d}t = 0$. This functional is related to $\mathcal{H}$ as $\mathcal{H}[\boldsymbol{\Upsilon} + \boldsymbol{v}'] - \mathcal{H}[\boldsymbol{\Upsilon}] = \mathcal{E}[\boldsymbol{v}'] + O(|\boldsymbol{v}'|^3)$. In this study, we regard $\mathcal{E}$ as the total wave energy of the system. It is noted that, when discussing wave–mean flow interaction processes, the total pseudoenergy, pseudo-momentum or wave action would be a more suitable choice as the invariant of the system. In any case, our analysis does not depend on the physical meaning of $\mathcal{E}$ so long as the system is governed by an equation written as (2.3). Please refer to Shepherd (1990) for the non-canonical Hamiltonian formulation (2.1) of various problems arising in geophysical fluid dynamics.

To simplify the problem, we have assumed that the reference state $\boldsymbol{\Upsilon}$ is the local minimum point of the Hamiltonian functional $\mathcal{H}$, which makes $\hat{\boldsymbol{A}}$ positive–definite. This is the necessary condition for $\mathcal{E} \geqslant 0$ and also a sufficient condition for the stability of the system (Shepherd 1990). Then, in the same way as the usual matrix calculation, we consider a factorisation of $\hat{\boldsymbol{A}}$; that is, we seek an operator $\hat{\boldsymbol{L}}$ that satisfies

$$\hat{\boldsymbol{A}} = \hat{\boldsymbol{L}}\hat{\boldsymbol{L}}^\dagger. \tag{2.4}$$

Let us suppose that this factorisation is achieved and, in addition, we find an inverse of $\hat{\boldsymbol{L}}$; namely, $\hat{\boldsymbol{L}}^{-1}$ that satisfies $\hat{\boldsymbol{L}}\hat{\boldsymbol{L}}^{-1} = \hat{\boldsymbol{L}}^{-1}\hat{\boldsymbol{L}} = \hat{\boldsymbol{I}}$ where $\hat{\boldsymbol{I}}$ is the identity operator. Then, redefining the state vector and the Hermitian operator as $\boldsymbol{\psi} = \hat{\boldsymbol{L}}^\dagger \boldsymbol{v}'/\sqrt{2}$ and $\hat{\boldsymbol{H}} = \hat{\boldsymbol{L}}^{-1}\hat{\boldsymbol{B}}\hat{\boldsymbol{L}}^{\dagger-1}$, we may further simplify (2.3) as

$$\mathrm{i}\frac{\partial \boldsymbol{\psi}}{\partial t} = \hat{\boldsymbol{H}}\boldsymbol{\psi}, \tag{2.5}$$

which is the most basic description for a linear system that conserves the energy norm $\mathcal{E} = \int |\boldsymbol{\psi}|^2 \mathrm{d}\boldsymbol{x}$.

https://doi.org/10.1017/jfm.2019.825 Published online by Cambridge University Press

2.2. *Wigner transform and pseudo-differential operator*

To seek an operator $\hat{\boldsymbol{L}}$ that satisfies the condition (2.4), here we use the Wigner transform. The Wigner transform is a kind of mapping that associates a linear operator with a function called the symbol, which is frequently used in theoretical physics to correspond a quantum system to a classical system (e.g. McDonald 1988; Gérard *et al.* 1997; Cohen 2012). When an operator acting on functional space is given, its Wigner transform is defined as follows: we first represent the operator in an integral transformation form,

$$\hat{\boldsymbol{F}}\boldsymbol{\phi}(\boldsymbol{x}) = \int \boldsymbol{F}(\boldsymbol{x}, \boldsymbol{x}')\boldsymbol{\phi}(\boldsymbol{x}')\,\mathrm{d}\boldsymbol{x}', \tag{2.6}$$

where $\boldsymbol{\phi}(\boldsymbol{x}) : \mathbb{R}^d \to \mathbb{C}^n$ is an arbitrary test function. Then, the Fourier transform of the kernel function with respect to the relative position of its arguments yields the symbol,

$$\boldsymbol{f}(\boldsymbol{x}, \boldsymbol{p}) = \int \boldsymbol{F}\left(\boldsymbol{x} + \frac{\boldsymbol{x}'}{2}, \boldsymbol{x} - \frac{\boldsymbol{x}'}{2}\right) \mathrm{e}^{-\mathrm{i}\boldsymbol{p}\cdot\boldsymbol{x}'/\mu}\,\mathrm{d}\boldsymbol{x}', \tag{2.7}$$

where the parameter μ, which corresponds to the Dirac constant in quantum mechanics, is introduced. Wavenumber is now represented by $\boldsymbol{p}$, which is distinguished from the usual definition $\boldsymbol{k}$ by a multiplication factor μ; i.e. one may understand that a relationship $\boldsymbol{p} = \mu\boldsymbol{k}$ holds. A symbol is a matrix-valued function defined on $\mathbb{R}^{2d}$. The operator $\hat{\boldsymbol{F}}$ is then represented using its symbol $\boldsymbol{f}(\boldsymbol{x}, \boldsymbol{p})$ as a kind of pseudo-differential operator,

$$\hat{\boldsymbol{F}}\boldsymbol{\phi}(\boldsymbol{x}) = \frac{1}{(2\pi\mu)^d} \iint \boldsymbol{f}\left(\frac{\boldsymbol{x} + \boldsymbol{x}'}{2}, \boldsymbol{p}\right) \boldsymbol{\phi}(\boldsymbol{x}')\mathrm{e}^{\mathrm{i}\boldsymbol{p}\cdot(\boldsymbol{x}-\boldsymbol{x}')/\mu}\,\mathrm{d}\boldsymbol{x}'\,\mathrm{d}\boldsymbol{p}, \tag{2.8}$$

which is rather simply denoted as $\hat{\boldsymbol{F}} = \boldsymbol{f}(\hat{\boldsymbol{x}}, \hat{\boldsymbol{p}})$. It is noted that, whereas the mapping from an operator to a function, $\hat{\boldsymbol{F}} \to \boldsymbol{f}(\boldsymbol{x}, \boldsymbol{p})$, is called the Wigner transform, its inverse, $\boldsymbol{f}(\boldsymbol{x}, \boldsymbol{p}) \to \hat{\boldsymbol{F}}$, is called the Weyl correspondence. In this study, we assume that $\mu \ll 1$ and all the symbols can be expanded in terms of μ; such as

$$\boldsymbol{f} = \boldsymbol{f}_0 + \mu\boldsymbol{f}_1 + \mu^2\boldsymbol{f}_2 + \cdots, \tag{2.9}$$

which are the same requirements as those for the usual WKBJ approximation.

The Wigner transform associates a product between operators, $\hat{\boldsymbol{F}}\hat{\boldsymbol{G}} = \boldsymbol{f}(\hat{\boldsymbol{x}}, \hat{\boldsymbol{p}})\boldsymbol{g}(\hat{\boldsymbol{x}}, \hat{\boldsymbol{p}})$, with an operation between their symbols, which is called the star product and denoted as $\boldsymbol{f}(\boldsymbol{x}, \boldsymbol{p}) \star \boldsymbol{g}(\boldsymbol{x}, \boldsymbol{p})$. As described in appendix A, we may explicitly expand the definition of the star product as follows:

$$\boldsymbol{f}(\boldsymbol{x}, \boldsymbol{p}) \star \boldsymbol{g}(\boldsymbol{x}, \boldsymbol{p}) = \sum_{\boldsymbol{m},\boldsymbol{n}} \frac{(-1)^{|\boldsymbol{n}|}}{\boldsymbol{m}!\boldsymbol{n}!} \left(\frac{\mathrm{i}\mu}{2}\right)^{|\boldsymbol{m}|+|\boldsymbol{n}|} \nabla_x^{\boldsymbol{m}}\nabla_p^{\boldsymbol{n}}\boldsymbol{f}(\boldsymbol{x}, \boldsymbol{p})\nabla_x^{\boldsymbol{n}}\nabla_p^{\boldsymbol{m}}\boldsymbol{g}(\boldsymbol{x}, \boldsymbol{p}). \tag{2.10}$$

Here, we have introduced non-negative integer vectors as $\boldsymbol{m} = (m_1, m_2, \ldots, m_d)$, $\boldsymbol{n} = (n_1, n_2, \ldots, n_d) \in \mathbb{N}_0^d$ and used the multi-index notation; $|\boldsymbol{m}| = m_1 + m_2 + \cdots + m_d$, $\boldsymbol{m}! = m_1!m_2!\cdots m_d!$, $\nabla_x^{\boldsymbol{m}} = \partial^{|\boldsymbol{m}|}/\partial x_1^{m_1}\partial x_2^{m_2}\cdots\partial x_d^{m_d}$, $\nabla_p^{\boldsymbol{m}} = \partial^{|\boldsymbol{m}|}/\partial p_1^{m_1}\partial p_2^{m_2}\cdots\partial p_d^{m_d}$. Summation in (2.10) is taken over all the combinations with respect to $\boldsymbol{m}$ and $\boldsymbol{n}$.

https://doi.org/10.1017/jfm.2019.825 Published online by Cambridge University Press

To make the expressions concise, let us further introduce a notation to specify the jth-order component in a function, such as for (2.9),

$$\overline{\boldsymbol{f}}^{j} = \boldsymbol{f}_j, \tag{2.11}$$

which enables the leading- and first-order terms in the star product to be written down as follows:

$$\overline{\boldsymbol{f} \star \boldsymbol{g}}^{0} = \boldsymbol{f}_0 \boldsymbol{g}_0 \tag{2.12a}$$

$$\begin{aligned} \overline{\boldsymbol{f} \star \boldsymbol{g}}^{1} &= \boldsymbol{f}_1 \boldsymbol{g}_0 + \boldsymbol{f}_0 \boldsymbol{g}_1 + \overline{\boldsymbol{f}_0 \star \boldsymbol{g}_0}^{1} \\ &= \boldsymbol{f}_1 \boldsymbol{g}_0 + \boldsymbol{f}_0 \boldsymbol{g}_1 + \frac{\mathrm{i}}{2} \sum_{i=1}^{d} \left(\frac{\partial \boldsymbol{f}_0}{\partial x_i} \frac{\partial \boldsymbol{g}_0}{\partial p_i} - \frac{\partial \boldsymbol{f}_0}{\partial p_i} \frac{\partial \boldsymbol{g}_0}{\partial x_i} \right). \end{aligned} \tag{2.12b}$$

2.3. *Factorisation and inversion of an operator*

Now we write the symbols of $\hat{\boldsymbol{A}}$ and $\hat{\boldsymbol{L}}$ in (2.4) as $\boldsymbol{a}(\boldsymbol{x}, \boldsymbol{p}) = \boldsymbol{a}_0 + \mu \boldsymbol{a}_1 + \cdots$, $\boldsymbol{l}(\boldsymbol{x}, \boldsymbol{p}) = \boldsymbol{l}_0 + \mu \boldsymbol{l}_1 + \cdots$, which makes (2.4) to be $\boldsymbol{a} = \boldsymbol{l} \star \boldsymbol{l}^{\dagger}$, or

$$\boldsymbol{a}_0 = \boldsymbol{l}_0 \boldsymbol{l}_0^{\dagger}, \tag{2.13a}$$

$$\begin{aligned} \boldsymbol{a}_1 &= \boldsymbol{l}_1 \boldsymbol{l}_0^{\dagger} + \boldsymbol{l}_0 \boldsymbol{l}_1^{\dagger} + \overline{\boldsymbol{l}_0 \star \boldsymbol{l}_0^{\dagger}}^{1} \\ &\vdots \end{aligned} \tag{2.13b}$$

Since $\hat{\boldsymbol{A}}$ has been assumed to be a positive–definite Hermitian operator, its symbol $\boldsymbol{a}(\boldsymbol{x}, \boldsymbol{p})$ must be a Hermitian matrix with its leading-order component, $\boldsymbol{a}_0$, positive–definite almost everywhere in $\mathbb{R}^{2d}$. Therefore, we may find $\boldsymbol{l}_0$ satisfying (2.13a) using the Cholesky factorisation algorithm, which ensures $\boldsymbol{l}_0$ is a lower triangular non-singular matrix. Then, the remaining components in $\boldsymbol{l}$ are successively found, such as

$$\boldsymbol{l}_1 = \tfrac{1}{2} (\boldsymbol{a}_1 - \overline{\boldsymbol{l}_0 \star \boldsymbol{l}_0^{\dagger}}^{1}) \boldsymbol{l}_0^{\dagger -1}. \tag{2.14}$$

In this way, we can make an operator $\hat{\boldsymbol{L}} = \boldsymbol{l}(\hat{\boldsymbol{x}}, \hat{\boldsymbol{p}})$ that factorises $\hat{\boldsymbol{A}}$ as (2.4).

Next, we consider an inverse operator of $\hat{\boldsymbol{L}}$. That is to say, we shall seek a symbol of $\hat{\boldsymbol{L}}^{-1}$ written as $\boldsymbol{l}^{I} = \boldsymbol{l}_0^{I} + \mu \boldsymbol{l}_1^{I} + \cdots$, which should be distinguished from the common inverse matrix $\boldsymbol{l}^{-1}$. Then, the equation to be solved becomes $\boldsymbol{I} = \boldsymbol{l} \star \boldsymbol{l}^{I}$, or

$$\boldsymbol{I} = \boldsymbol{l}_0 \boldsymbol{l}_0^{I}, \tag{2.15a}$$

$$\begin{aligned} 0 &= \boldsymbol{l}_1 \boldsymbol{l}_0^{I} + \boldsymbol{l}_0 \boldsymbol{l}_1^{I} + \overline{\boldsymbol{l}_0 \star \boldsymbol{l}_0^{I}}^{1} \\ &\vdots, \end{aligned} \tag{2.15b}$$

where $\boldsymbol{I}$ is the identity matrix. Equation (2.15a) is immediately solved as $\boldsymbol{l}_0^{I} = \boldsymbol{l}_0^{-1}$. The remaining parts in $\boldsymbol{l}^{I}$ are successively obtained, such as

$$\boldsymbol{l}_1^{I} = -\boldsymbol{l}_0^{-1} (\boldsymbol{l}_1 \boldsymbol{l}_0^{I} + \overline{\boldsymbol{l}_0 \star \boldsymbol{l}_0^{I}}^{1}). \tag{2.16}$$

It is noted that the associative law of the star product ensures that $\boldsymbol{I} = \boldsymbol{l} \star \boldsymbol{l}^{I}$ is equivalent to $\boldsymbol{I} = \boldsymbol{l}^{I} \star \boldsymbol{l}$. In this way, we derive $\hat{\boldsymbol{L}}^{-1} = \boldsymbol{l}^{I}(\hat{\boldsymbol{x}}, \hat{\boldsymbol{p}})$, an inverse of $\hat{\boldsymbol{L}}$. Inverse of an operator is generally found by this method as long as the leading-order component of its symbol is non-singular.

https://doi.org/10.1017/jfm.2019.825 Published online by Cambridge University Press

2.4. *Diagonalisation of an operator*

Now that we obtain operators $\hat{\boldsymbol{L}}$ and $\hat{\boldsymbol{L}}^{-1}$ that enable the equation of motion (2.3) to be transformed into (2.5), and next we seek an operator $\hat{\boldsymbol{U}} = \boldsymbol{u}(\hat{\boldsymbol{x}}, \hat{\boldsymbol{p}})$ that diagonalises $\hat{\boldsymbol{H}} = \boldsymbol{h}(\hat{\boldsymbol{x}}, \hat{\boldsymbol{p}})$ into $\hat{\boldsymbol{U}}\hat{\boldsymbol{H}}\hat{\boldsymbol{U}}^{-1} = \hat{\boldsymbol{\Omega}} = \mathrm{diag}(\hat{\Omega}_1, \hat{\Omega}_2, \ldots, \hat{\Omega}_n) = \boldsymbol{\omega}(\hat{\boldsymbol{x}}, \hat{\boldsymbol{p}})$; i.e.

$$\boldsymbol{u} \star \boldsymbol{h} \star \boldsymbol{u}^I = \boldsymbol{\omega} = \begin{pmatrix} \omega_1(\boldsymbol{x}, \boldsymbol{p}) & 0 & \ldots & 0 \\ 0 & \omega_2(\boldsymbol{x}, \boldsymbol{p}) & & \vdots \\ \vdots & & \ddots & 0 \\ 0 & \ldots & 0 & \omega_n(\boldsymbol{x}, \boldsymbol{p}) \end{pmatrix}. \tag{2.17}$$

If we replace the star product in (2.17) by the algebraic product, the problem becomes the usual eigenvalue problem. In that case, the diagonal elements of $\boldsymbol{\omega}$ coincide with the dispersion relations obtained from a crude manner where the spatial gradient in the coefficient parameter is ignored. As discussed in § 1, the dispersion relations of IGWs and RWs cannot be derived simultaneously in this way; i.e. evaluation of the higher-order terms in (2.17) is required to derive the proper dispersion relation of RWs. Perturbation analysis of the equation (2.17) was first conducted by Littlejohn & Flynn (1991), who excluded the possibility that the leading-order eigenvalues are degenerate. Here we follow their method with some additional remarks on the situation when the degenerate modes are separated in their perturbation terms.

As a preparation, we expand $\boldsymbol{h}, \boldsymbol{\omega}, \boldsymbol{u}, \boldsymbol{u}^I$ and rewrite $\boldsymbol{u}$ and $\boldsymbol{u}^I$ in the following forms:

$$\boldsymbol{u} = \left(\boldsymbol{I} - \frac{\mu}{2} \overline{\boldsymbol{u}_0 \star \boldsymbol{u}_0^{-1}}^1 + \mu \boldsymbol{\alpha} \right) \boldsymbol{u}_0 + O(\mu^2) \tag{2.18a}$$

$$\boldsymbol{u}^I = \boldsymbol{u}_0^{-1} \left(\boldsymbol{I} - \frac{\mu}{2} \overline{\boldsymbol{u}_0 \star \boldsymbol{u}_0^{-1}}^1 - \mu \boldsymbol{\alpha} \right) + O(\mu^2). \tag{2.18b}$$

Accordingly, the leading- and first-order terms in (2.17) become

$$\boldsymbol{u}_0 \boldsymbol{h}_0 \boldsymbol{u}_0^{-1} = \boldsymbol{\omega}_0, \tag{2.19}$$

and

$$\overline{\boldsymbol{u}_0 \star \boldsymbol{h} \star \boldsymbol{u}_0^{-1}}^1 - \tfrac{1}{2} \overline{\boldsymbol{u}_0 \star \boldsymbol{u}_0^{-1}}^1 \boldsymbol{\omega}_0 - \tfrac{1}{2} \boldsymbol{\omega}_0 \overline{\boldsymbol{u}_0 \star \boldsymbol{u}_0^{-1}}^1 + \boldsymbol{\alpha}\boldsymbol{\omega}_0 - \boldsymbol{\omega}_0 \boldsymbol{\alpha} = \boldsymbol{\omega}_1. \tag{2.20}$$

To simplify the problem, the eigenvalue equation (2.19) is assumed to be solvable in the usual algebraic manner, thus excluding the possibility that the geometric multiplicity in the leading-order matrix prevents the diagonalisation. We then seek the solutions $\boldsymbol{\alpha}$, $\boldsymbol{\omega}_1$ for (2.20). Problems are classified into two cases depending on whether the leading-order eigenvalues in $\boldsymbol{\omega}_0$ are degenerate or not.

We first consider the non-degenerate case when all the diagonal elements in $\boldsymbol{\omega}_0(\boldsymbol{x}, \boldsymbol{p})$, which we write $(\omega_{0,1}, \omega_{0,2}, \ldots, \omega_{0,n})$, take different values. In the following, the kth row and lth column element in a matrix is denoted by a subscript (k, l). Let us take the kth diagonal element in (2.20) to derive

$$\boldsymbol{\omega}_{1(k,k)} = [\overline{\boldsymbol{u}_0 \star \boldsymbol{h} \star \boldsymbol{u}_0^{-1}}^1]_{(k,k)} - \omega_{0,k} [\overline{\boldsymbol{u}_0 \star \boldsymbol{u}_0^{-1}}^1]_{(k,k)}. \tag{2.21}$$

Similarly, taking a non-diagonal element (k, l) in (2.20) yields

$$\boldsymbol{\alpha}_{(k,l)} = \frac{1}{\omega_{0,k} - \omega_{0,l}} [\overline{\boldsymbol{u}_0 \star \boldsymbol{h} \star \boldsymbol{u}_0^{-1}}^1]_{(k,l)} - \frac{1}{2} \frac{\omega_{0,k} + \omega_{0,l}}{\omega_{0,k} - \omega_{0,l}} [\overline{\boldsymbol{u}_0 \star \boldsymbol{u}_0^{-1}}^1]_{(k,l)}. \tag{2.22}$$

https://doi.org/10.1017/jfm.2019.825 Published online by Cambridge University Press

Diagonal elements of $\boldsymbol{\alpha}$ can be arbitrarily chosen in each calculation, as is usual in the perturbation theory of eigenvalue analysis (see, e.g. Sakurai & Napolitano 2011). It may be convenient to let all of them be 0.

Next, we consider the degenerate case when some of the diagonal elements in $\boldsymbol{\omega}_0(\boldsymbol{x}, \boldsymbol{p})$ take the same value. In this case, the denominators in (2.22) will vanish, leading to the perturbation theory breaking down. Therefore, we must take an alternative approach. As is shown in the following, the perturbation term $\boldsymbol{\alpha}$ is determinable only if proper conditions are satisfied in the leading order. In degenerate cases, $\boldsymbol{\omega}_0$ can be written in a block-diagonalised form as

$$\boldsymbol{\omega}_0 = \begin{pmatrix} \boldsymbol{\omega}_0^1 & \mathbf{0} & \dots & \mathbf{0} \\ \mathbf{0} & \boldsymbol{\omega}_0^2 & & \vdots \\ \vdots & & \ddots & \mathbf{0} \\ \mathbf{0} & \dots & \mathbf{0} & \boldsymbol{\omega}_0^r \end{pmatrix}, \tag{2.23}$$

where $\boldsymbol{\omega}_0^b = \omega_0^b \boldsymbol{I}$ $(1 \leqslant b \leqslant r)$ are scalar matrices of some dimensions and ω_0^b all take different values (hereafter superscript b indicates the bth block-diagonal elements). In the present case, $\boldsymbol{u}_0$ cannot be determined uniquely from the leading-order equation; even when a solution $\boldsymbol{u}_0$ of (2.19) is found, transformation

$$\boldsymbol{u}_0'(\boldsymbol{x}, \boldsymbol{p}) = \boldsymbol{s}(\boldsymbol{x}, \boldsymbol{p}) \boldsymbol{u}_0(\boldsymbol{x}, \boldsymbol{p}), \tag{2.24}$$

with an arbitrary block-diagonalised non-singular matrix

$$\boldsymbol{s} = \begin{pmatrix} \boldsymbol{s}^1 & \mathbf{0} & \dots & \mathbf{0} \\ \mathbf{0} & \boldsymbol{s}^2 & & \vdots \\ \vdots & & \ddots & \mathbf{0} \\ \mathbf{0} & \dots & \mathbf{0} & \boldsymbol{s}^r \end{pmatrix}, \tag{2.25}$$

retains $\boldsymbol{u}_0'$ as the solution of (2.19). Consequently, the problem reduces to the need to specify $\boldsymbol{s}$ such that the higher-order equations are consistently solved. Extracting the bth block-diagonal element from (2.20) with $\boldsymbol{u}_0$ replaced by $\boldsymbol{u}_0'$ yields

$$[\overline{\boldsymbol{u}_0' \star \boldsymbol{h} \star \boldsymbol{u}_0'^{-1}}^{1}]^b - \omega_0^b [\overline{\boldsymbol{u}_0' \star \boldsymbol{u}_0'^{-1}}^{1}]^b = \boldsymbol{\omega}_1^b. \tag{2.26}$$

Because this equation involves the derivatives of $\boldsymbol{s}^b$, which originates from the factor $\overline{\boldsymbol{s}^b \star \cdots}^{1}$, partial differential equations have to be solved to specify $\boldsymbol{s}^b$ and $\boldsymbol{\omega}_1^b$. That is to say, degeneracy cannot generally be resolved quasi-locally. This trouble has already been pointed out in a classical study (Littlejohn & Flynn 1991) and emerges in electromagnetic waves or elastic waves whose polarised modes are degenerate (see, e.g. Ryzhik *et al.* 1996). However, if the degenerate eigenvalue ω_0^b is identically 0, which is indeed the case for the dispersion relations of barotropic and baroclinic RWs in a stratified fluid, (2.26) reduces to the following form:

$$\boldsymbol{s}^b [\overline{\boldsymbol{u}_0 \star \boldsymbol{h} \star \boldsymbol{u}_0^{-1}}^{1}]^b \boldsymbol{s}^{b-1} = \boldsymbol{\omega}_1^b. \tag{2.27}$$

Since this is a purely algebraic problem, we may find the eigenvalues $\boldsymbol{\omega}_1^b = \mathrm{diag}(\omega_{1,1}^b, \omega_{1,2}^b, \dots)$ and the corresponding eigenvectors $\boldsymbol{s}^b$. Moving on to $\boldsymbol{\alpha}$, let

https://doi.org/10.1017/jfm.2019.825 Published online by Cambridge University Press

us decompose it into block-diagonal elements and non-block-diagonal elements; $\boldsymbol{\alpha} = \boldsymbol{\alpha}^B + \boldsymbol{\alpha}^N$. Non-block-diagonal elements $\boldsymbol{\alpha}^N$ are immediately obtained as in the non-degenerate case from (2.20). As for $\boldsymbol{\alpha}^B$, or equivalently $\boldsymbol{\alpha}^b$, after some algebraic manipulation, one may find from the $O(\mu^2)$ terms in (2.17) the following expression:

$$\boldsymbol{\alpha}^b_{(k,l)} = \frac{1}{\omega^b_{1,k} - \omega^b_{1,l}} \left[\overline{\tilde{\boldsymbol{u}} \star \boldsymbol{h} \star \tilde{\boldsymbol{u}}^I}^2 \right]^b_{(k,l)}, \tag{2.28}$$

where

$$\tilde{\boldsymbol{u}} \equiv \left(\boldsymbol{I} - \frac{\mu}{2} \overline{\boldsymbol{u}'_0 \star \boldsymbol{u}'^{-1}_0}^1 + \mu \boldsymbol{\alpha}^N \right) \boldsymbol{u}'_0 \tag{2.29a}$$

$$\tilde{\boldsymbol{u}}^I \equiv \boldsymbol{u}'^{-1}_0 \left(\boldsymbol{I} - \frac{\mu}{2} \overline{\boldsymbol{u}'_0 \star \boldsymbol{u}'^{-1}_0}^1 - \mu \boldsymbol{\alpha}^N \right), \tag{2.29b}$$

are known variables.

Although not described in detail here, when the diagonalisation (2.17) is completed within $O(\mu)$ terms, the higher-order terms in $\boldsymbol{u}$ and $\boldsymbol{\omega}$ can be successively derived by extending the perturbation expansion. The diagonalisation procedure constructed here is valid no matter whether $\boldsymbol{h}$ is Hermitian or not. In the special case when $\boldsymbol{h}$ is Hermitian, $\hat{\boldsymbol{U}}$ can be chosen as a unitary operator and $\boldsymbol{\omega}(\boldsymbol{x}, \boldsymbol{p})$ becomes a real matrix, as is easily verified to at least $O(\mu)$ accuracy by taking the complex conjugate of the expressions so far and, in fact, ascertainable up to any order. These properties ensure the energy conservation of the system, which we shall see in the following.

Let us go back to (2.5). Transforming the state vector as $\boldsymbol{\psi}' = \hat{\boldsymbol{U}}\boldsymbol{\psi}$ changes it to

$$\mathrm{i} \frac{\partial \boldsymbol{\psi}'}{\partial t} = \hat{\boldsymbol{\Omega}} \boldsymbol{\psi}', \tag{2.30}$$

which is a set of n independent equations, whose ith element is specifically

$$\mathrm{i} \frac{\partial \psi'_i}{\partial t} = \omega_i(\hat{\boldsymbol{x}}, \hat{\boldsymbol{p}}) \psi'_i. \tag{2.31}$$

This equation is in the same form as the Schrödinger equation where ω_i is interpreted as the Hamiltonian with its arguments, $\hat{\boldsymbol{x}}$ and $\hat{\boldsymbol{p}}$, respectively corresponding to the position and momentum operators. Then, as can be shown from the traditional WKBJ analysis (see appendix B), the real function $\omega_i(\boldsymbol{x}, \boldsymbol{p})$ specifies the dispersion relation of the ith mode, to at least $O(\mu)$ accuracy. The ith column of $\boldsymbol{u}^\dagger(\boldsymbol{x}, \boldsymbol{p})$, which is the symbol of the eigenoperator $\hat{\boldsymbol{U}}^\dagger$, can be interpreted as the polarisation relation of the ith mode. These two relations are characterised in a quasi-local sense; although $\boldsymbol{\omega}(\boldsymbol{x}, \boldsymbol{p})$ and $\boldsymbol{u}(\boldsymbol{x}, \boldsymbol{p})$ are defined at each point $(\boldsymbol{x}, \boldsymbol{p}) \in \mathbb{R}^{2d}$, they are derived by taking the gradients in the coefficient parameters into account. Their physical interpretations, namely the frequency and the oscillation angle of the medium, are visualised when we envisage a finite-sized wave packet with a local wavenumber $\boldsymbol{p}$ in the vicinity of $\boldsymbol{x}$.

The scalar function $\psi_i(\boldsymbol{x}, t)$ represents the complex wave signal associated with the ith mode. It should be noted that the local energy density, which is originally defined as $|\boldsymbol{\psi}(\boldsymbol{x})|^2$, and its transformed counterpart, $|\boldsymbol{\psi}'(\boldsymbol{x})|^2 = \sum_i |\psi'_i(\boldsymbol{x})|^2$, do not necessarily coincide. However, the unitarity of the eigenoperator $\hat{\boldsymbol{U}}$ ensures that the total energy of the system, $\mathcal{E} = \int |\boldsymbol{\psi}(\boldsymbol{x})|^2 \, \mathrm{d}\boldsymbol{x}$, is equivalent to its transformed counterpart, $\mathcal{E}' = \int |\boldsymbol{\psi}'(\boldsymbol{x})|^2 \, \mathrm{d}\boldsymbol{x}$. Hence, we may fairly interpret $|\psi'_i(\boldsymbol{x})|^2$ as the energy density of the ith mode. Furthermore, the reality condition of $\omega_i(\boldsymbol{x}, \boldsymbol{p})$ ensures $\omega_i(\hat{\boldsymbol{x}}, \hat{\boldsymbol{p}})$ is Hermitian and, therefore, according to (2.31), the energy of each mode, e.g. $\int |\psi'_i(\boldsymbol{x})|^2 \, \mathrm{d}\boldsymbol{x}$ for the ith component, is individually conserved.

https://doi.org/10.1017/jfm.2019.825 Published online by Cambridge University Press

2.5. *Transport theory*

In the following, we take a particular mode i and omit the prime and subscripts of ψ_i' and ω_i. We then introduce a linear operator $\hat{W}$ corresponding to ψ such that

$$\hat{W}\phi(\boldsymbol{x}) \equiv \psi(\boldsymbol{x}) \int \psi^\dagger(\boldsymbol{x}')\phi(\boldsymbol{x}')\,\mathrm{d}\boldsymbol{x}' \tag{2.32}$$

holds for any other test function $\phi(\boldsymbol{x})$. In quantum mechanics, $\hat{W}$ and its corresponding symbol $w(\boldsymbol{x},\boldsymbol{p})$ are called the density operator and the Wigner distribution function, respectively (Kubo 1964). The latter is explicitly written as

$$w(\boldsymbol{x},\boldsymbol{p}) = \int \psi\left(\boldsymbol{x}+\frac{\boldsymbol{x}'}{2}\right)\psi^\dagger\left(\boldsymbol{x}-\frac{\boldsymbol{x}'}{2}\right)\mathrm{e}^{-\mathrm{i}\boldsymbol{p}\cdot\boldsymbol{x}'/\mu}\,\mathrm{d}\boldsymbol{x}'. \tag{2.33}$$

Notably, the useful relationships,

$$\frac{1}{(2\pi\mu)^d}\int w(\boldsymbol{x},\boldsymbol{p})\,\mathrm{d}\boldsymbol{p} = |\psi(\boldsymbol{x})|^2 \tag{2.34a}$$

$$\int w(\boldsymbol{x},\boldsymbol{p})\,\mathrm{d}\boldsymbol{x} = |\tilde{\psi}(\boldsymbol{p})|^2 \tag{2.34b}$$

hold, where $\tilde{\psi}(\boldsymbol{p}) = \int \psi(\boldsymbol{x})\mathrm{e}^{-\mathrm{i}\boldsymbol{p}\cdot\boldsymbol{x}/\mu}\,\mathrm{d}\boldsymbol{x}$, and therefore the total energy of this mode coincides with

$$\frac{1}{(2\pi\mu)^d}\iint w(\boldsymbol{x},\boldsymbol{p})\,\mathrm{d}\boldsymbol{x}\,\mathrm{d}\boldsymbol{p}. \tag{2.35}$$

These expressions indicate that the Wigner distribution function w can be interpreted as the energy density in physical and wavenumber space. From (2.5), the governing equation for the density operator and the Wigner distribution function are respectively derived as

$$\mathrm{i}\frac{\partial\hat{W}}{\partial t} = \hat{\Omega}\hat{W} - \hat{W}\hat{\Omega} \quad \text{and} \quad \mathrm{i}\frac{\partial w}{\partial t} = \omega\star w - w\star\omega, \tag{2.36a,b}$$

which are sometimes referred to as the von Neumann equations (Petruccione & Breuer 2002). In the same way as Powell & Vanneste (2005), we expand the latter part of (2.36) with respect to μ to obtain

$$\frac{\partial w}{\partial t} + \mu\boldsymbol{\nabla}_p\omega\cdot\boldsymbol{\nabla}_x w - \mu\boldsymbol{\nabla}_x\omega\cdot\boldsymbol{\nabla}_p w = O(\mu^3), \tag{2.37}$$

or equivalently,

$$\frac{\partial w}{\partial t} + \mu\boldsymbol{\nabla}_x\cdot(\boldsymbol{c}_x w) + \mu\boldsymbol{\nabla}_p\cdot(\boldsymbol{c}_p w) = O(\mu^3), \tag{2.38}$$

where $(\boldsymbol{c}_x, \boldsymbol{c}_p) = (\boldsymbol{\nabla}_p\omega, -\boldsymbol{\nabla}_x\omega)$ is the gradient of the dispersion relation, and hence represents the group velocity defined in $(\boldsymbol{x},\boldsymbol{p})$ space. When we neglect the higher-order terms in (2.38), it reduces to the special case of the transport equation (1.2) with no source or sink term.

https://doi.org/10.1017/jfm.2019.825 Published online by Cambridge University Press

3. Example: shallow water model

3.1. *Formulation*

The shallow water equation is the simplest model suitable for the current analysis. In this model, the wave and vortical modes coexist and their properties change due to the effect of spatial variations in the coefficient parameters. Let us define the Hamiltonian of the system,

$$\mathcal{H} = \int \left(\frac{hu^2 + hv^2}{2} + \frac{g(h+D)^2}{2} \right) \mathrm{d}\boldsymbol{x}, \tag{3.1}$$

where $\boldsymbol{x} = (x, y)^{\mathrm{T}}$ is the horizontal coordinate and $u(\boldsymbol{x}, t)$, $v(\boldsymbol{x}, t)$ and $h(\boldsymbol{x}, t)$ represent the zonal velocity, meridional velocity and the thickness of the water, respectively. The acceleration due to gravity g is constant whereas the bottom topography $D(\boldsymbol{x})$ varies in space. The equation of motion is represented as

$$\begin{pmatrix} \partial u/\partial t \\ \partial v/\partial t \\ \partial h/\partial t \end{pmatrix} = \begin{pmatrix} 0 & f/h & -\partial_x \\ -f/h & 0 & -\partial_y \\ -\partial_x & -\partial_y & 0 \end{pmatrix} \begin{pmatrix} \delta\mathcal{H}/\delta u \\ \delta\mathcal{H}/\delta v \\ \delta\mathcal{H}/\delta h \end{pmatrix}, \tag{3.2}$$

where $f(y)$ is the Coriolis parameter varying in the meridional direction and ∂_x and ∂_y represent the partial derivatives with respect to x and y, respectively.

The steady solution of (3.2) that corresponds to the state of rest is

$$u = 0, \quad v = 0, \quad h = H(\boldsymbol{x}) \equiv H_0 - D(\boldsymbol{x}), \tag{3.3a–c}$$

where H_0 is a constant. Since this solution is a local minimum of $\mathcal{H}$, the equation of motion linearised around it belongs to the class considered in § 2. Let us write the equation in the same form as (2.3),

$$\mathrm{i} \begin{pmatrix} H & 0 & 0 \\ 0 & H & 0 \\ 0 & 0 & g \end{pmatrix} \begin{pmatrix} \partial u/\partial t \\ \partial v/\partial t \\ \partial \eta/\partial t \end{pmatrix} = \begin{pmatrix} 0 & \mathrm{i}fH & -\mathrm{i}gH\partial_x \\ -\mathrm{i}fH & 0 & -\mathrm{i}gH\partial_y \\ -\mathrm{i}g\partial_x H & -\mathrm{i}g\partial_y H & 0 \end{pmatrix} \begin{pmatrix} u \\ v \\ \eta \end{pmatrix}, \tag{3.4}$$

where the surface displacement $\eta \equiv h - H$ is defined. We then introduce the WKBJ parameter μ and replace the spatial derivatives as $(\partial_x, \partial_y) \to \mu(\partial_x, \partial_y)$. Note that the parameter μ is here used for bookkeeping purposes and will be regarded as unity in the numerical analysis (§ 3.2). Following the concept in (2.4), we redefine variables as $\boldsymbol{\psi} = (\sqrt{H/2}u, \sqrt{H/2}v, \sqrt{g/2}\eta)^{\mathrm{T}}$. Further introducing the parameter representing the gravity wave speed, $c = \sqrt{gH}$, and its derivatives, $\boldsymbol{\nabla}_x c = (c_x, c_y)$, we rewrite (3.4) in the form of (2.5), or $\mathrm{i}\partial\boldsymbol{\psi}/\partial t = \boldsymbol{h}(\hat{\boldsymbol{x}}, \hat{\boldsymbol{p}})\boldsymbol{\psi}$, with

$$\boldsymbol{h} = \underbrace{\begin{pmatrix} 0 & \mathrm{i}f & -cp_x \\ -\mathrm{i}f & 0 & -cp_y \\ -cp_x & -cp_y & 0 \end{pmatrix}}_{\boldsymbol{h}_0} + \mu \underbrace{\begin{pmatrix} 0 & 0 & \dfrac{\mathrm{i}c_x}{2} \\ 0 & 0 & \dfrac{\mathrm{i}c_y}{2} \\ -\dfrac{\mathrm{i}c_x}{2} & -\dfrac{\mathrm{i}c_y}{2} & 0 \end{pmatrix}}_{\boldsymbol{h}_1}, \tag{3.5}$$

where the zonal and meridional wavenumbers are defined: $\boldsymbol{p} = (p_x, p_y)^{\mathrm{T}}$. As is apparent, matrices $\boldsymbol{h}_0$ and $\boldsymbol{h}_1$ are both Hermitian. Therefore we may find a unitary operator

https://doi.org/10.1017/jfm.2019.825 Published online by Cambridge University Press

$\boldsymbol{u}(\hat{\boldsymbol{x}}, \hat{\boldsymbol{p}})$ that diagonalises $\boldsymbol{h}(\hat{\boldsymbol{x}}, \hat{\boldsymbol{p}})$ as $\boldsymbol{u} \star \boldsymbol{h} \star \boldsymbol{u}^\dagger = \boldsymbol{\omega}$. Its leading-order component is immediately found by solving the equation $\boldsymbol{u}_0 \boldsymbol{h}_0 \boldsymbol{u}_0^\dagger = \boldsymbol{\omega}_0$ as

$$\boldsymbol{u}_0 = \begin{pmatrix} \dfrac{\theta p_x - \mathrm{i} f p_y}{\sqrt{2}\theta p} & \dfrac{\theta p_y + \mathrm{i} f p_x}{\sqrt{2}\theta p} & \dfrac{cp}{\sqrt{2}\theta} \\ \dfrac{-\theta p_x - \mathrm{i} f p_y}{\sqrt{2}\theta p} & \dfrac{-\theta p_y + \mathrm{i} f p_x}{\sqrt{2}\theta p} & \dfrac{cp}{\sqrt{2}\theta} \\ \dfrac{\mathrm{i} c p_y}{\theta} & \dfrac{-\mathrm{i} c p_x}{\theta} & \dfrac{f}{\theta} \end{pmatrix}, \tag{3.6}$$

where $p \equiv \sqrt{p_x^2 + p_y^2}$ and $\theta(\boldsymbol{x}, \boldsymbol{p}) \equiv \sqrt{f^2 + c^2 p^2}$. The corresponding eigenvalues are specified by the diagonal elements of

$$\boldsymbol{\omega}_0 = \begin{pmatrix} \sqrt{f^2 + c^2 p^2} & 0 & 0 \\ 0 & -\sqrt{f^2 + c^2 p^2} & 0 \\ 0 & 0 & 0 \end{pmatrix}, \tag{3.7}$$

which exhibit the basic dispersion relations of IGWs and stationary vortices. Next, we analyse the perturbation of these dispersion relations induced by the topographic slope and the planetary β-effect.

In accordance with (2.21), the first-order terms of the dispersion relations $\boldsymbol{\omega}_1$ correspond to the diagonal elements of

$$\begin{aligned} &\boldsymbol{u}_0 \boldsymbol{h}_1 \boldsymbol{u}_0^\dagger \\ &\quad + \frac{\mathrm{i}}{2}\left(\frac{\partial \boldsymbol{u}_0}{\partial x}\frac{\partial \boldsymbol{h}_0}{\partial p_x}\boldsymbol{u}_0^\dagger - \frac{\partial \boldsymbol{u}_0}{\partial p_x}\frac{\partial \boldsymbol{h}_0}{\partial x}\boldsymbol{u}_0^\dagger + \frac{\partial \boldsymbol{u}_0}{\partial y}\frac{\partial \boldsymbol{h}_0}{\partial p_y}\boldsymbol{u}_0^\dagger - \frac{\partial \boldsymbol{u}_0}{\partial p_y}\frac{\partial \boldsymbol{h}_0}{\partial y}\boldsymbol{u}_0^\dagger \right) \\ &\quad + \frac{\mathrm{i}}{2}\left(\boldsymbol{u}_0\frac{\partial \boldsymbol{h}_0}{\partial x}\frac{\partial \boldsymbol{u}_0^\dagger}{\partial p_x} - \boldsymbol{u}_0\frac{\partial \boldsymbol{h}_0}{\partial p_x}\frac{\partial \boldsymbol{u}_0^\dagger}{\partial x} + \boldsymbol{u}_0\frac{\partial \boldsymbol{h}_0}{\partial y}\frac{\partial \boldsymbol{u}_0^\dagger}{\partial p_y} - \boldsymbol{u}_0\frac{\partial \boldsymbol{h}_0}{\partial p_y}\frac{\partial \boldsymbol{u}_0^\dagger}{\partial y} \right) \\ &\quad + \frac{\mathrm{i}}{2}\left(\frac{\partial \boldsymbol{u}_0}{\partial x}\boldsymbol{h}_0\frac{\partial \boldsymbol{u}_0^\dagger}{\partial p_x} - \frac{\partial \boldsymbol{u}_0}{\partial p_x}\boldsymbol{h}_0\frac{\partial \boldsymbol{u}_0^\dagger}{\partial x} + \frac{\partial \boldsymbol{u}_0}{\partial y}\boldsymbol{h}_0\frac{\partial \boldsymbol{u}_0^\dagger}{\partial p_y} - \frac{\partial \boldsymbol{u}_0}{\partial p_y}\boldsymbol{h}_0\frac{\partial \boldsymbol{u}_0^\dagger}{\partial y} \right) \\ &\quad - \frac{\mathrm{i}\boldsymbol{\omega}_0}{2}\left(\frac{\partial \boldsymbol{u}_0}{\partial x}\frac{\partial \boldsymbol{u}_0^\dagger}{\partial p_x} - \frac{\partial \boldsymbol{u}_0}{\partial p_x}\frac{\partial \boldsymbol{u}_0^\dagger}{\partial x} + \frac{\partial \boldsymbol{u}_0}{\partial y}\frac{\partial \boldsymbol{u}_0^\dagger}{\partial p_y} - \frac{\partial \boldsymbol{u}_0}{\partial p_y}\frac{\partial \boldsymbol{u}_0^\dagger}{\partial y} \right). \end{aligned} \tag{3.8}$$

To obtain the $O(\mu)$ terms in the dispersion relation, we need only the $O(1)$ terms of the polarisation $\boldsymbol{u}$. This character is the same as that in the elementary perturbation theory of quantum mechanics (Sakurai & Napolitano 2011).

Consequently, we obtain the dispersion relations $\boldsymbol{\omega} = \mathrm{diag}(\omega_1, \omega_2, \omega_3)$ up to the $O(\mu)$ terms as

$$\omega_1 = \sqrt{f^2 + c^2 p^2} - \mu\left[\frac{\beta p_x (2f^2 + c^2 p^2)}{2p^2 (f^2 + c^2 p^2)} + \frac{fc(p_x c_y - p_y c_x)}{f^2 + c^2 p^2} \right] + O(\mu^2), \tag{3.9a}$$

$$\omega_2 = -\sqrt{f^2 + c^2 p^2} - \mu\left[\frac{\beta p_x (2f^2 + c^2 p^2)}{2p^2 (f^2 + c^2 p^2)} + \frac{fc(p_x c_y - p_y c_x)}{f^2 + c^2 p^2} \right] + O(\mu^2), \tag{3.9b}$$

$$\omega_3 = \frac{\mu c(-\beta c p_x + 2f p_x c_y - 2f p_y c_x)}{f^2 + c^2 p^2} + O(\mu^2), \tag{3.9c}$$

https://doi.org/10.1017/jfm.2019.825 Published online by Cambridge University Press

which govern the temporal change in the complex signals $\boldsymbol{\psi}' = (\psi_1', \psi_2', \psi_3')^{\mathrm{T}} = \boldsymbol{u}(\hat{\boldsymbol{x}}, \hat{\boldsymbol{p}})\boldsymbol{\psi}$ as

$$\mathrm{i}\frac{\partial \psi_i'}{\partial t} = \omega_i(\hat{\boldsymbol{x}}, \hat{\boldsymbol{p}})\psi_i', \quad i = 1, 2, 3. \tag{3.10}$$

It is noted that the tedious calculation (3.8) was conducted using Maxima, a free computer algebra system. The first two elements (3.9*a*,*b*), which satisfy $\omega_1(\boldsymbol{x}, \boldsymbol{p}) = -\omega_2(\boldsymbol{x}, -\boldsymbol{p})$, represent the dispersion relations for the complex conjugate pair of IGW modes: $\psi_1' = \psi_2'^{\dagger}$. Their $O(\mu)$ terms, which represent perturbation in the dispersion relation (see appendix B), cause the frequencies of IGWs to depend slightly on the propagation direction. This result is consistent with the WKBJ analysis by McKee (1973) for the case of $\beta = 0$, and a similar feature is also well known for the equatorial IGWs, whose dispersion relation depends on the propagation direction on the zonal axis (Matsuno 1966). The third element (3.9*c*) coincides with the famous dispersion relation of RWs (Pedlosky 1987).

Additionally, the group velocities of IGWs and RWs in physical space are derived as

$$\nabla_p \omega_1 = \begin{pmatrix} \dfrac{c^2 p_x}{\sqrt{f^2 + c^2 p^2}} \\ \dfrac{c^2 p_y}{\sqrt{f^2 + c^2 p^2}} \end{pmatrix} + O(\mu), \tag{3.11a}$$

$$\nabla_p \omega_3 = \mu \begin{pmatrix} \dfrac{-\beta c^2 + 2fcc_y}{f^2 + c^2 p^2} - \dfrac{2c^3 p_x(-\beta c p_x + 2f p_x c_y - 2f p_y c_x)}{(f^2 + c^2 p^2)^2} \\ -\dfrac{2fcc_x}{f^2 + c^2 p^2} - \dfrac{2c^3 p_y(-\beta c p_x + 2f p_x c_y - 2f p_y c_x)}{(f^2 + c^2 p^2)^2} \end{pmatrix} + O(\mu^2), \tag{3.11b}$$

where the $O(\mu)$ terms for IGWs are omitted. These expressions will be used for the flux analysis in § 3.2.

3.2. *Application to a numerical model*

The advantage of the current method is that the formulae derived using pseudo-differential operators are applicable to data produced by numerical atmosphere or ocean models. To demonstrate this, a simple numerical simulation for the propagation of IGWs and RWs in a shallow water model that solves (3.4) is conducted. To facilitate the analysis, we employ the easiest geometry, i.e. a rectangular domain with x and y both ranging from $-\pi$ to π, with double-periodic boundary conditions, neglecting the planetary β-effect such that f is constant. Suitable scaling yields constant parameters equal to unity; $f = g = 1$. The Arakawa C-gird is adopted (Haidvogel & Beckmann 1999), in which the variables u, v, η are evaluated at different grid points (figure 1). The total number of grid points in the model is $3 \times N_x \times N_y = 3 \times 128 \times 128$. The time integration is performed using the leapfrog scheme.

The bottom topography is

$$H(x, y) = 1.0 \times 10^{-2} - \frac{7.5 \times 10^{-3}(1 + \cos x)(1 + \cos y)}{4}, \tag{3.12}$$

https://doi.org/10.1017/jfm.2019.825 Published online by Cambridge University Press

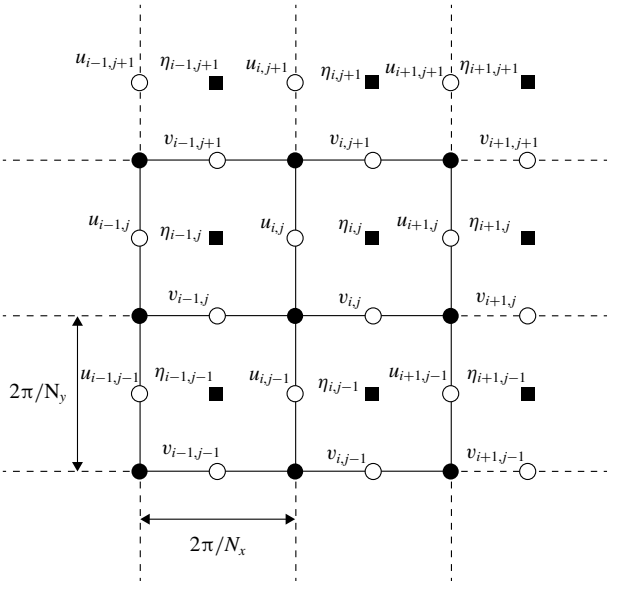


FIGURE 1. The staggered grids used in the numerical model. Because variables u, v, η are evaluated at different points, the phase shift for each wavenumber component has to be taken into account, as described in (3.17).

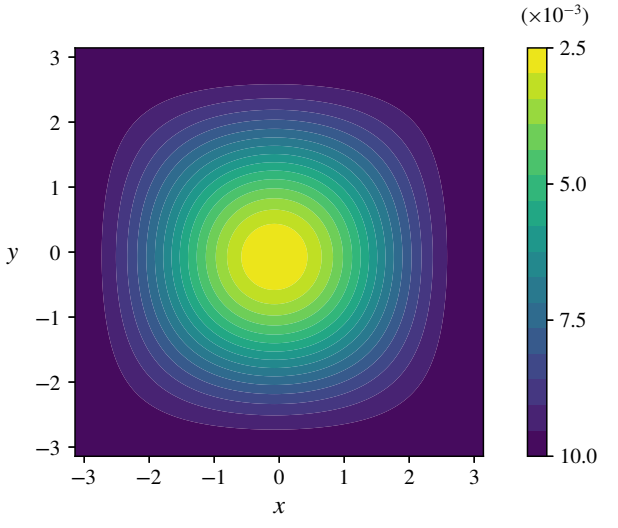


FIGURE 2. Water depth $H(x, y)$ in the numerical model. The bright area in the centre of the domain corresponds to the shallow region.

as depicted in figure 2. A localised wave packet,

$$\eta = 1.0 \times 10^{-5} \exp\left(-\frac{x^2 + (y + \pi/2)^2}{2(\pi/6)^2}\right) \sin(8.0x), \quad u = 0,\ v = 0, \tag{3.13}$$

https://doi.org/10.1017/jfm.2019.825 Published online by Cambridge University Press

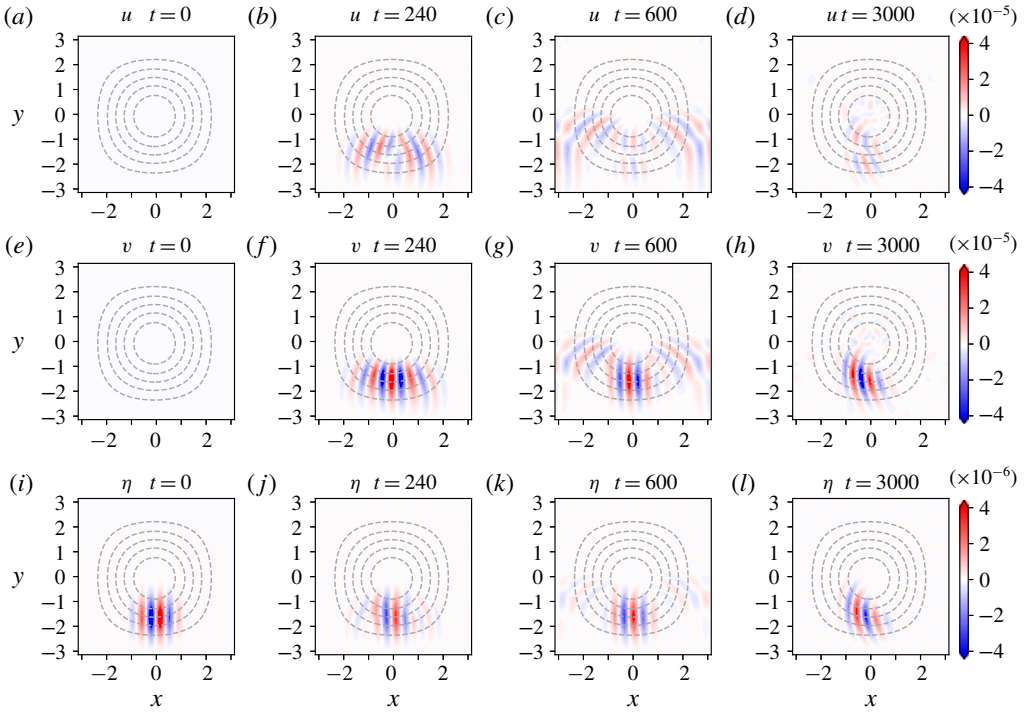


FIGURE 3. Results of the numerical simulation. (*a–d*) Zonal velocity u, (*e–h*) meridional velocity v and (*i–l*) surface elevation η are shown at $t = 0, 240, 600, 3000$. Dashed curves are contours of the reference depth $H(x, y)$. The rapidly propagating inertia–gravity wave and the slowly propagating Rossby wave are overlapping.

is arranged as the initial state and then allowed to propagate freely in the domain. Figure 3 shows a time series of the flow field. As the basic geostrophic adjustment, a pair of IGWs are immediately radiated away in opposite directions from the initial packet zone, whereas part of the flow field is left behind, almost retaining the geostrophic balance. This quasi-geostrophic flow pattern will also propagate leftward as an RW. This result suggests that the initial flow field was composed of a superposition of two distinguished wave modes, the IGW and the RW. The main objective is to decompose these modes and analyse their properties independently.

To achieve this goal, we need to prepare a discrete form of the pseudo-differential operator (2.8). In general, formulae for operations among symbols based on star products can be constructed up to the infinite order of μ. However, for practical purposes we must truncate a perturbation series at a finite order. The first-order truncation is the most convenient choice because it enables the application of fast Fourier transform (FFT) in the calculation of the pseudo-differential operator.

First, by taking the 'central difference' with respect to $\boldsymbol{x}$ and $\boldsymbol{x}'$, we separate (2.8) approximately into two parts as

$$\boldsymbol{f}(\hat{\boldsymbol{x}}, \hat{\boldsymbol{p}})\boldsymbol{\phi} = \frac{\boldsymbol{\xi}(\boldsymbol{x}) + \boldsymbol{\zeta}(\boldsymbol{x})}{2} + O(\mu^2), \tag{3.14}$$

https://doi.org/10.1017/jfm.2019.825 Published online by Cambridge University Press

where

$$\boldsymbol{\xi}(\boldsymbol{x}) \equiv \frac{1}{(2\pi\mu)^d} \iint \boldsymbol{f}(\boldsymbol{x}, \boldsymbol{p})\boldsymbol{\phi}(\boldsymbol{x}')\mathrm{e}^{\mathrm{i}\boldsymbol{p}\cdot(\boldsymbol{x}-\boldsymbol{x}')/\mu}\,\mathrm{d}\boldsymbol{p}\,\mathrm{d}\boldsymbol{x}', \tag{3.15a}$$

$$\boldsymbol{\zeta}(\boldsymbol{x}) \equiv \frac{1}{(2\pi\mu)^d} \iint \boldsymbol{f}(\boldsymbol{x}', \boldsymbol{p})\boldsymbol{\phi}(\boldsymbol{x}')\mathrm{e}^{\mathrm{i}\boldsymbol{p}\cdot(\boldsymbol{x}-\boldsymbol{x}')/\mu}\,\mathrm{d}\boldsymbol{p}\,\mathrm{d}\boldsymbol{x}'. \tag{3.15b}$$

Then, as in the usual discrete Fourier transform, we discretise these factors as

$$\boldsymbol{\xi}_{ij} = \sum_{k=-N_x/2+1}^{N_x/2} \sum_{l=-N_y/2+1}^{N_y/2} \boldsymbol{f}_{ijkl}\tilde{\boldsymbol{\phi}}_{kl}\mathrm{e}^{2\pi\mathrm{i}(ki/N_x+lj/N_y)}, \tag{3.16a}$$

$$\tilde{\boldsymbol{\phi}}_{kl} = \frac{1}{N_xN_y} \sum_{i=-N_x/2+1}^{N_x/2} \sum_{j=-N_y/2+1}^{N_y/2} \boldsymbol{\phi}_{ij}\mathrm{e}^{-2\pi\mathrm{i}(ki/N_x+lj/N_y)}, \tag{3.16b}$$

$$\boldsymbol{\zeta}_{ij} = \sum_{k=-N_x/2+1}^{N_x/2} \sum_{l=-N_y/2+1}^{N_y/2} \tilde{\boldsymbol{\zeta}}_{kl}\mathrm{e}^{2\pi\mathrm{i}(ki/N_x+lj/N_y)}, \tag{3.16c}$$

$$\tilde{\boldsymbol{\zeta}}_{kl} = \frac{1}{N_xN_y} \sum_{i=-N_x/2+1}^{N_x/2} \sum_{j=-N_y/2+1}^{N_y/2} \boldsymbol{f}_{ijkl}\boldsymbol{\phi}_{ij}\mathrm{e}^{-2\pi\mathrm{i}(ki/N_x+lj/N_y)}. \tag{3.16d}$$

Because (3.16*b*) and (3.16*c*) are in the standard form of discrete Fourier transforms, they are calculable by FFT. In the current model, the variables u, v, η are evaluated at different points (figure 1). Therefore, a phase shift for each wavenumber component is taken into account; i.e. the discrete Fourier transform for each variable of $\boldsymbol{\psi} = (\sqrt{H/2}u, \sqrt{H/2}v, \sqrt{g/2}\eta)^{\mathrm{T}}$ is redefined as

$$\tilde{\psi}_{1kl} = \frac{1}{N_xN_y} \sum_{i=-N_x/2+1}^{N_x/2} \sum_{j=-N_y/2+1}^{N_y/2} \psi_{1ij}\mathrm{e}^{-2\pi\mathrm{i}(k(i-1/2)/N_x+lj/N_y)}, \tag{3.17a}$$

$$\tilde{\psi}_{2kl} = \frac{1}{N_xN_y} \sum_{i=-N_x/2+1}^{N_x/2} \sum_{j=-N_y/2+1}^{N_y/2} \psi_{2ij}\mathrm{e}^{-2\pi\mathrm{i}(ki/N_x+l(j-1/2)/N_y)}, \tag{3.17b}$$

$$\tilde{\psi}_{3kl} = \frac{1}{N_xN_y} \sum_{i=-N_x/2+1}^{N_x/2} \sum_{j=-N_y/2+1}^{N_y/2} \psi_{3ij}\mathrm{e}^{-2\pi\mathrm{i}(ki/N_x+lj/N_y)}, \tag{3.17c}$$

and the exponents in (3.16*b*) and (3.16*d*) are replaced in the same manner. Using the symbol of the unitary operator, equation (3.6), we perform the linear transformation, $\boldsymbol{\psi}' = (\psi_g, \psi_g^{\dagger}, \psi_r)^{\mathrm{T}} \equiv \boldsymbol{u}(\hat{\boldsymbol{x}}, \hat{\boldsymbol{p}})\boldsymbol{\psi}$, to obtain the complex signals of IGWs and RWs, respectively. (Although (3.14) involves $O(\mu)$ terms, because the symbol of the unitary operator $\boldsymbol{u}$ is prepared only in the $O(1)$ term, the result obtained is of leading-order accuracy. It is noted that the first-order correction of $\boldsymbol{u}$ is too complicated to be written down explicitly, but its computation could be done by separately preparing the symbol matrices that composes (2.22) and combining them.) Figure 4 shows the real and imaginary parts of the complex signals ψ_g and ψ_r. The two wave modes are successfully decomposed by this method.

https://doi.org/10.1017/jfm.2019.825 Published online by Cambridge University Press

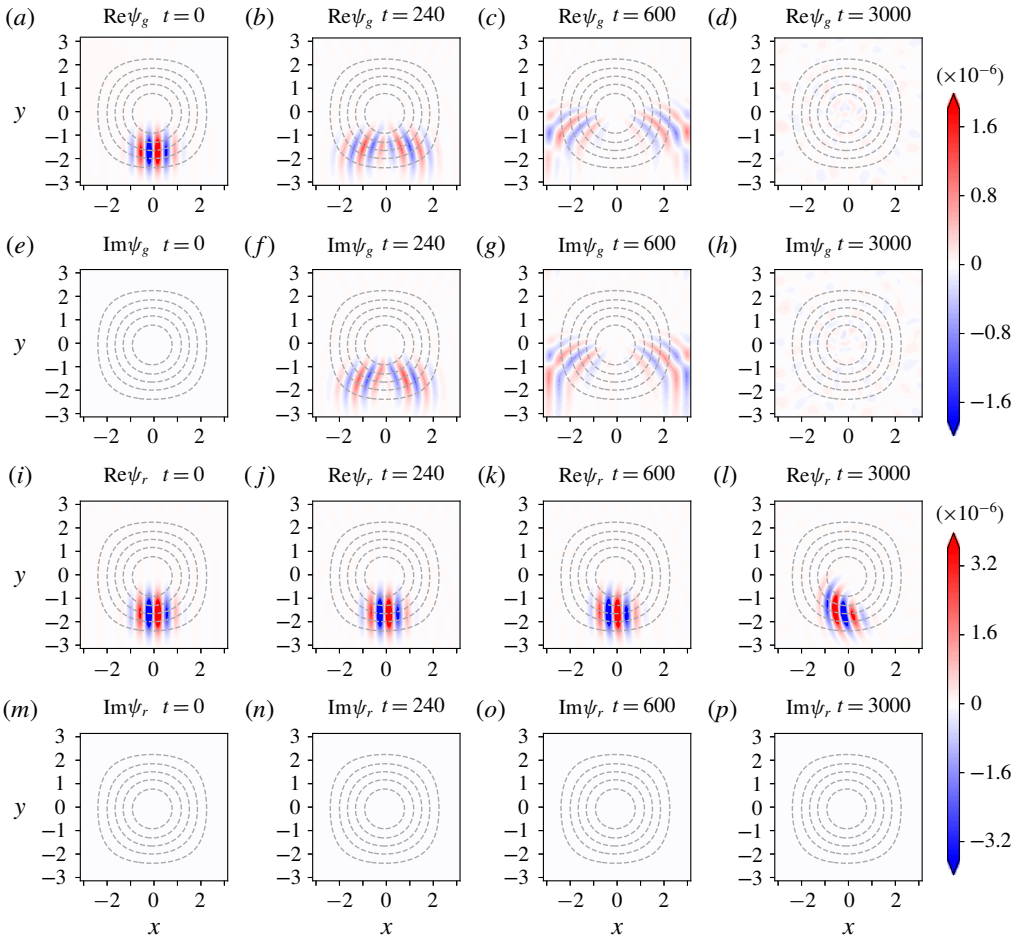


FIGURE 4. Complex signals for the inertia–gravity wave and the Rossby wave, denoted as ψ_g and ψ_r, respectively. (*a–d*) Real parts of ψ_g, (*e–h*) imaginary parts of ψ_g, (*i–l*) real parts of ψ_r and (*m–p*) imaginary parts of ψ_r are shown at $t = 0, 240, 600, 3000$. Note that the imaginary parts of ψ_r vanish for reasons that are explained in the text.

Next, we discretise the Wigner distribution function, $w(\boldsymbol{x}, \boldsymbol{p})$ as defined in (2.33). In this study, we adopt the discretised Wigner distribution function that corresponds to a discretised complex signal ψ_{ij} as

$$w_{ijkl} = \frac{4}{N_x N_y} \sum_{i'=-N_x/2+1}^{N_x/2} \sum_{j'=-N_y/2+1}^{N_y/2} \psi_{i+i'j+j'} \psi^{\dagger}_{i-i'j-j'} \mathrm{e}^{-4\pi \mathrm{i}(ki'/N_x + lj'/N_y)}, \tag{3.18}$$

where indices of ψ, $\psi^{\dagger}$ are extended outside the domain taking advantage of the periodic boundary conditions. Expression (3.18) satisfies the total energy condition,

$$\sum_{i=-N_x/2+1}^{N_x/2} \sum_{j=-N_y/2+1}^{N_y/2} |\psi_{ij}|^2 = \sum_{i=-N_x/2+1}^{N_x/2} \sum_{j=-N_y/2+1}^{N_y/2} \sum_{k=-N_x/4+1}^{N_x/4} \sum_{l=-N_y/4+1}^{N_y/4} w_{ijkl}. \tag{3.19}$$

https://doi.org/10.1017/jfm.2019.825 Published online by Cambridge University Press

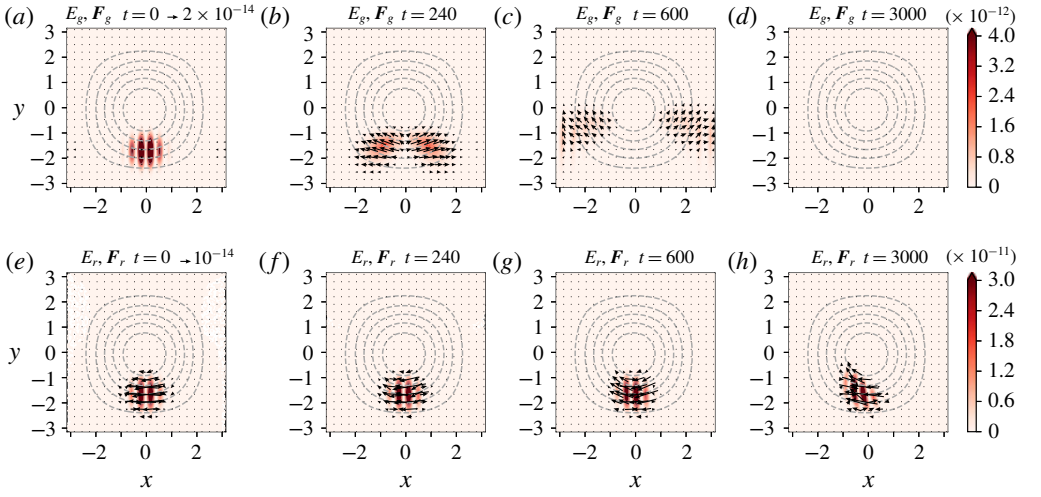


FIGURE 5. Energy density and (vector) fluxes for (*a–d*) the inertia–gravity wave and (*e–h*) the Rossby wave at $t=0, 240, 600, 3000$. A spatially oscillating structure arises in the case of the Rossby wave.

In this definition, the maximum wavenumber of the Wigner distribution function becomes half the Nyquist wavenumber. To avoid this inconvenience, other definitions for the discrete Wigner distribution function have been suggested (Chassande-Mottin & Pai 2005), although these are not discussed in detail here.

Projecting the transport equation (2.38) onto physical space, we define the energy density, $E(\boldsymbol{x}) = (2\pi\mu)^{-2} \int w \,\mathrm{d}\boldsymbol{p}$, and its flux, $\boldsymbol{F}(\boldsymbol{x}) = (2\pi\mu)^{-2} \int \boldsymbol{c}_x w \,\mathrm{d}\boldsymbol{p}$. Their discretised forms are

$$E_{ij} = \sum_{k=-N_x/4+1}^{N_x/4} \sum_{l=-N_y/4+1}^{N_y/4} w_{ijkl}, \tag{3.20a}$$

$$\boldsymbol{F}_{ij} = \sum_{k=-N_x/4+1}^{N_x/4} \sum_{l=-N_y/4+1}^{N_y/4} \boldsymbol{c}_{ijkl} w_{ijkl}, \tag{3.20b}$$

where $\boldsymbol{c}_{ijkl}$ is the group velocity of each wave specified in (3.11). Energy density and flux are calculated using these expressions and depicted in figure 5, which exhibits the wave energy propagation associated with each mode. However, the energy density and flux of the RW oscillate with the half-length of its wave packet, reflecting the phase variation in the signal. Such a feature is not seen in the case of IGWs except for the initial time (figures 4*a*,*e* and 5*a*) when the two-way propagating wave packets are overlapping. Historically, the phase dependence of the flux of RWs has been recognised as a nuisance by atmospheric scientists and overcome such as by Plumb (1985) and Takaya & Nakamura (2001). While these studies heuristically derived phase-independent representations of the pseudo-momentum flux associated with RWs, here we offer a more systematic consideration to solve this problem.

What causes the differences between IGWs and RWs? Why do only RWs exhibit an oscillating energy density in this analysis? A simple answer can be found when focusing on their dispersion relations. As (3.9*c*) shows, the dispersion relation of RWs

https://doi.org/10.1017/jfm.2019.825 Published online by Cambridge University Press

is an odd function with respect to wavenumber; i.e. $\omega(\boldsymbol{x},\boldsymbol{p}) = -\omega(\boldsymbol{x},-\boldsymbol{p})$ holds. In this case, a solution of

$$\mathrm{i}\frac{\partial\psi}{\partial t} = \omega(\hat{\boldsymbol{x}},\hat{\boldsymbol{p}})\psi \tag{3.21}$$

is also a solution of

$$\mathrm{i}\frac{\partial\psi^{\dagger}}{\partial t} = \omega(\hat{\boldsymbol{x}},\hat{\boldsymbol{p}})\psi^{\dagger}. \tag{3.22}$$

Therefore, we can assume a solution satisfying $\psi = \psi^{\dagger}$; i.e. ψ can be a real function. In figure 4, it is indeed seen that the complex signal of the RW, ψ_r, possesses only the real part, whereas that of the IGWs, ψ_g, has both the real and imaginary parts, which is a consequence of the dispersion relation of IGWs not being an odd function. As inferred from the contrasting expressions, $|\cos x|^2 = (1+\cos 2x)/2$ and $|\mathrm{e}^{\mathrm{i}x}|^2 = 1$, energy and flux of the real RW signals always oscillate but those of the complex IGW signals do not.

This oscillatory structure of the RW can be removed by introducing a filtering technique. Using the Heaviside function $V(x)$ that satisfies $V(x) = 0$ for $x < 0$ and $V(x) = 1$ for $x > 0$, let us define a symbol $v_\omega(\boldsymbol{x},\boldsymbol{p}) = V(\omega(\boldsymbol{x},\boldsymbol{p}))$. Then, the operator $v_\omega(\hat{\boldsymbol{x}},\hat{\boldsymbol{p}})$ acts as a filter that transmits only the positive frequency components. As is obvious from its definition, $v_\omega(\hat{\boldsymbol{x}},\hat{\boldsymbol{p}})$ commutes with $\omega(\hat{\boldsymbol{x}},\hat{\boldsymbol{p}})$; $v_\omega(\hat{\boldsymbol{x}},\hat{\boldsymbol{p}})\omega(\hat{\boldsymbol{x}},\hat{\boldsymbol{p}}) = \omega(\hat{\boldsymbol{x}},\hat{\boldsymbol{p}})v_\omega(\hat{\boldsymbol{x}},\hat{\boldsymbol{p}})$. From this property, the operation of $v_\omega(\hat{\boldsymbol{x}},\hat{\boldsymbol{p}})$ on (3.21) yields

$$\mathrm{i}\frac{\partial}{\partial t}(v_\omega(\hat{\boldsymbol{x}},\hat{\boldsymbol{p}})\psi) = \omega(\hat{\boldsymbol{x}},\hat{\boldsymbol{p}})(v_\omega(\hat{\boldsymbol{x}},\hat{\boldsymbol{p}})\psi), \tag{3.23}$$

which means that $v_\omega(\hat{\boldsymbol{x}},\hat{\boldsymbol{p}})\psi$ is also a solution of the original equation (3.21) and, moreover, it possesses both the real and imaginary parts. Figure 6 shows the filtered RW signal $\psi_r' \equiv v_\omega(\hat{\boldsymbol{x}},\hat{\boldsymbol{p}})\psi_r$ and its associated energy density and flux. Both the real and imaginary parts of ψ_r' appear and the oscillatory structure of the energy density and flux is eliminated. It is noted that this filtering method resembles that in Sato, Kinoshita & Okamoto (2013). In Sato *et al.* (2013), the filtering function is defined in zonal wavenumber space by assuming a zonally symmetric background field, whereas the method presented here is a more general approach because it adaptively takes account of the local dispersion relation that varies from place to place.

4. Discussion and conclusions

This paper develops a general theoretical framework for wave decomposition in a slowly varying medium. The Wigner transform, which links an operator to a function, and its associated pseudo-differential operator provide a good perspective on this issue. Based on the asymptotic expansion of pseudo-differential operators, we construct a procedure to decompose a linearised fluid system into mutually independent wave signals, each of which is governed by a single wave equation $\mathrm{i}\partial\psi/\partial t = \omega(\hat{\boldsymbol{x}},\hat{\boldsymbol{p}})\psi$. During this, the polarisation relations $\boldsymbol{u}(\boldsymbol{x},\boldsymbol{p})$ and the dispersion relations $\boldsymbol{\omega}(\boldsymbol{x},\boldsymbol{p})$ are systematically derived up to any order of accuracy. According to the formulation in § 2, this decomposition is possible if either of the following two conditions is satisfied:

(i) The leading-order dispersion relations are non-degenerate.
(ii) The leading-order dispersion relations of degenerate modes are identically 0 and resolved in the first order.

https://doi.org/10.1017/jfm.2019.825 Published online by Cambridge University Press

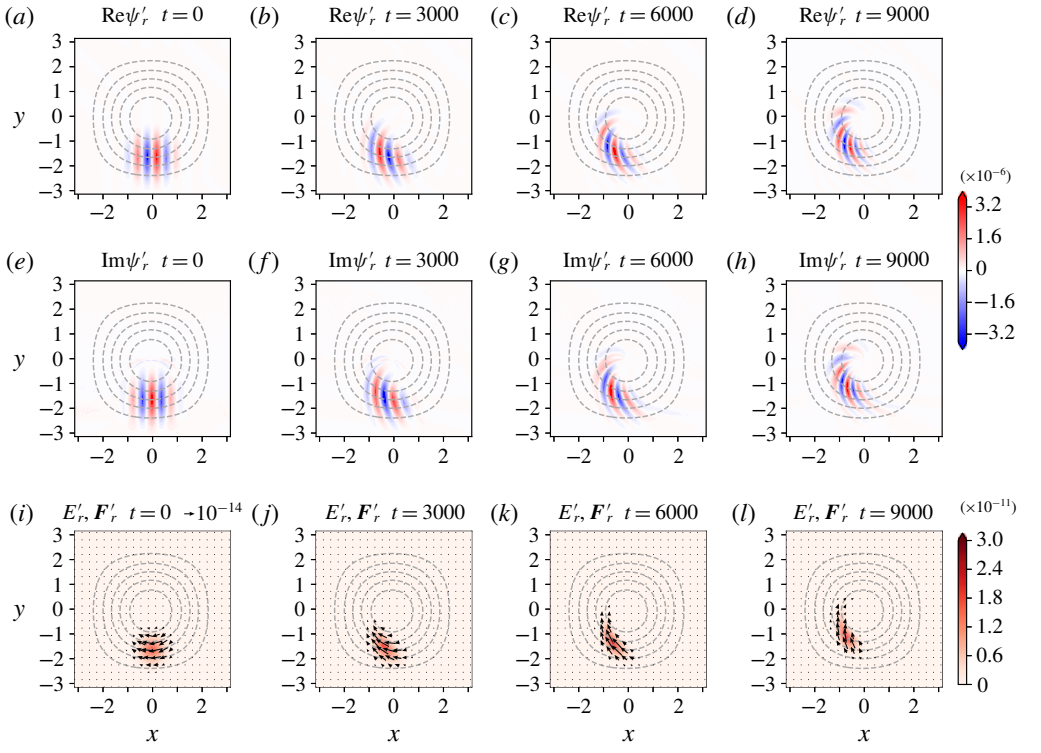


FIGURE 6. (*a–d*) Real parts and (*e–h*) imaginary parts of the filtered complex signal of the Rossby wave, $\psi'_r = v_\omega(\hat{\boldsymbol{x}}, \hat{\boldsymbol{p}})\psi_r$, and (*i–l*) its associated energy density E'_r and flux $\boldsymbol{F}'_r$ at $t = 0, 3000, 6000, 9000$. Note that times t are different from those in the previous figures.

Some types of waves, such as electromagnetic waves or elastic waves, do not belong to these classes; degenerate polarised modes cannot be decomposed quasi-locally. The classical transport theory, therefore, takes account of the correlation of degenerate modes (Ryzhik *et al.* 1996). However, typical waves in the ocean and atmosphere, such as sound waves, IGWs and RWs, are decomposable. It is particularly noteworthy that barotropic and baroclinic RWs in a stratified fluid are degenerate as the zero-frequency mode in the leading-order description, but decomposed in the $O(\mu)$ terms.

The main content of the paper is the presentation of a practical method to diagnose flux of energy (or other conserved quantities) possessed by each wave signal, making use of the transport theory applied to model output data. The flux derived in the current approach satisfies the group velocity property $\boldsymbol{F} \sim E\boldsymbol{c}_g$ in the plane-wave limit, where $\boldsymbol{F}$, E and $\boldsymbol{c}_g$ are energy flux, energy density and group velocity, respectively. A filtering method is also introduced, which ensures the phase independence of energy density and its flux even for RWs. To the author's best knowledge, this study is the first to separately analyse the fluxes associated with IGWs and RWs in one model with a solid theoretical basis. It is noted that, if we compose the Wigner distribution function numerically, $N_x^2 \times N_y^2$ ($\times$ time steps) variables have to be stored in the two-dimensional case. However, for the practical purpose of visualising the energy flux in physical or wavenumber space, what we need is the energy density and flux projected onto each space, such as E_{ij} and $\boldsymbol{F}_{ij}$ in (3.20). They can be calculated at each grid point, (i, j), separately. Therefore, we actually do not need a large computer memory.

https://doi.org/10.1017/jfm.2019.825 Published online by Cambridge University Press

Here, we discuss the difference between the present method and some relevant works. First, the study of wave–vortex decomposition has a long history. Most of the works have focused on the effect from nonlinear couplings (e.g. Machenhauer 1977; Warn *et al.* 1995; Vanneste 2013; Yasuda, Sato & Sugimoto 2015; Chouksey, Eden & Brüggemann 2018), where the vortex component is specifically named the 'balanced' mode. Asymptotic expansion with respect to the Rossby or Froude number has revealed how nonlinearity modifies the balanced mode. This study, on the other hand, considers the corrections of the linear polarisation and dispersion relations of every mode due to inhomogeneity based on asymptotic expansion with respect to the WKBJ parameter. Extending the current study to the cases of finite-amplitude waves will be an important future work. Second, one may find other types of linear wave–vortex decomposition using a numerical eigenvalue analysis. For example, Žagar *et al.* (2015) offered numerical decomposition of IGWs and RWs with the use of eigenfunction expansion on a sphere. This type of method is effective to analyse waves with spatial scales comparable with the size of a closed domain. The current method, on the other hand, is inherently applicable to local wave packets existing in an infinite domain. Third, the classical transport theory has incorporated effect from inhomogeneity of a medium as scattering terms (Powell & Vanneste 2005). The present method can also include the scattering effect into the formulation if we take account of rapid variations in the coefficient parameters. It is expected that a future study will also evaluate the scattering terms using model output data in the presence of, e.g. small-scale random topography.

Finally, the location of this study in a wide class of ray theory is considered. In the conventional ray-tracing method, propagation of wave action density is described by the equations $\partial A/\partial t + \boldsymbol{\nabla}_x \cdot (\dot{\boldsymbol{x}} A) = 0$, $\dot{\boldsymbol{x}} = \boldsymbol{\nabla}_k \omega$, and $\dot{\boldsymbol{k}} = -\boldsymbol{\nabla}_x \omega$, where the dispersion relation $\omega(\boldsymbol{x}, \boldsymbol{k})$ should be preliminarily given (Lighthill 1978). The current study offers a formulation which is valid one order higher than the conventional studies; the dispersion relation involves $O(\mu)$ terms which is meaningful in the transport equation (2.38) with $O(\mu^2)$ accuracy, whereas the classical ray tracing involves only the leading-order terms in the dispersion relation, which makes the action conservation equation of $O(\mu)$ (Whitham 1970; Vanneste & Shepherd 1999). This study rationalises that the shift of dispersion relation caused by the gradients in parameters can become meaningful in ray tracing, which is the case for RWs or even for IGWs in a frontal area, as has been pointed out in § 1.

Although this study applies the developed techniques only to the energy analysis of IGWs and RWs in a simple shallow water model, their pseudo-momentum and its associated residual volume transport will also be accessible in the same manner by computing the displacements of fluid parcels based on the velocity and frequency data and applying them to the generalised Lagrangian mean formulation (Bühler 2014). Application to a stratified fluid with background mean flow is another important step. The methodology can also be extended to forced–dissipative systems, as noted in appendix C, as well as including scattering effect. The new wave decomposition method introduced here will become useful as a data diagnostic technique for various situations in atmospheric and oceanic research.

Acknowledgements

The author expresses his gratitude to H. Aiki, N. Zhao and two anonymous reviewers for their invaluable comments on the original manuscript. Fruitful discussions with S. Inagaki, Y. Kosuga and M. Sasaki are also gratefully acknowledged.

https://doi.org/10.1017/jfm.2019.825 Published online by Cambridge University Press

This study was supported by JSPS KAKENHI grant number JP16H02226 and the Collaborative Research Program of Research Institute for Applied Mechanics, Kyushu University. The numerical model code of the shallow water equation was originally developed by C.-H. Kim and J.-H. Yoon.

Appendix A. Derivation of the star product

Looking back on the definition of the Wigner transform (2.8), one may first find the representation of the star product as

$$\boldsymbol{f}(\boldsymbol{x},\boldsymbol{p})\star\boldsymbol{g}(\boldsymbol{x},\boldsymbol{p}) = \frac{1}{(\pi\mu)^{2d}}\iiiint \boldsymbol{f}(\boldsymbol{x}+\boldsymbol{x}',\boldsymbol{p}+\boldsymbol{p}')\boldsymbol{g}(\boldsymbol{x}+\boldsymbol{x}'',\boldsymbol{p}+\boldsymbol{p}'')\mathrm{e}^{2\mathrm{i}(\boldsymbol{p}''\cdot\boldsymbol{x}'-\boldsymbol{p}'\cdot\boldsymbol{x}'')/\mu}\,\mathrm{d}\boldsymbol{x}'\,\mathrm{d}\boldsymbol{x}''\,\mathrm{d}\boldsymbol{p}'\,\mathrm{d}\boldsymbol{p}''. \tag{A 1}$$

It may be worth noting that (A 1) exhibits the associative law of the star product; $(\boldsymbol{f}\star\boldsymbol{g})\star\boldsymbol{h}=\boldsymbol{f}\star(\boldsymbol{g}\star\boldsymbol{h})$. Using the conventional formula

$$\frac{1}{2\pi\mu}\iint x^n p^m \mathrm{e}^{\mathrm{i}px/\mu}\,\mathrm{d}x\,\mathrm{d}p = \begin{cases}(\mathrm{i}\mu)^n n! & (n=m)\\ 0 & (n\neq m),\end{cases} \tag{A 2}$$

which combined with Taylor expansion leads to

$$\frac{1}{2\pi\mu}\iint f(x+x',p+p')\mathrm{e}^{\mathrm{i}p'x'/\mu}\,\mathrm{d}x'\,\mathrm{d}p' = \sum_{n=0}^{\infty}\frac{(\mathrm{i}\mu)^n}{n!}\frac{\partial^{2n}f(x,p)}{\partial_x^n\partial_p^n}, \tag{A 3}$$

equation (A 1) can be expanded with respect to μ to yield (2.10).

Appendix B. Accuracy of the dispersion relation

In § 2, we have shown that the dispersion relation $\omega(\boldsymbol{x},\boldsymbol{p})$ is derived by diagonalising $\boldsymbol{h}(\boldsymbol{x},\boldsymbol{p})$ that specifies the time evolution of the system. The dispersion relation that is obtained generally involves infinite number of terms expanded in a power series with respect to μ. A question then arises as to whether or not the higher-order components in ω are meaningful in view of the actual wave property. The traditional WKBJ analysis offers a clear answer to this question. Let us consider a single (pseudo-)differential equation

$$\mathrm{i}\frac{\partial\psi}{\partial t} = \omega(\hat{\boldsymbol{x}},\hat{\boldsymbol{p}})\psi, \tag{B 1}$$

and seek its solution with a single frequency, $\psi(\boldsymbol{x},t)=\tilde{\psi}(\boldsymbol{x})\mathrm{e}^{-\mathrm{i}\sigma t}$. Substitution of this in (B 1) yields

$$(\sigma-\omega(\hat{\boldsymbol{x}},\hat{\boldsymbol{p}}))\tilde{\psi}(\boldsymbol{x})=0. \tag{B 2}$$

Here we assume that the symbol $\omega(\boldsymbol{x},\boldsymbol{p})$ is a real function and also that the frequency σ is a real number. These are expanded with respect to μ as

$$\omega=\omega_0+\mu\omega_1+\cdots, \tag{B 3a}$$

$$\sigma=\sigma_0+\mu\sigma_1+\cdots. \tag{B 3b}$$

https://doi.org/10.1017/jfm.2019.825 Published online by Cambridge University Press

As in the usual manner of the WKBJ approximation, we consider a solution with its exponent expanded with respect to μ as

$$\begin{aligned}\tilde{\psi}(\boldsymbol{x}) &= \exp\left(\frac{1}{\mu}\phi(\boldsymbol{x})\right)\\ &= \exp\left\{\frac{1}{\mu}(\mathrm{i}\phi_0(\boldsymbol{x})+\mu(\phi_1^r(\boldsymbol{x})+\mathrm{i}\phi_1^i(\boldsymbol{x}))+\cdots)\right\},\end{aligned} \tag{B 4}$$

where $\phi_0, \phi_j^r, \phi_j^i$ are real functions. The imaginary part of the exponent,

$$\Theta(\boldsymbol{x}) \equiv \phi_0 + \mu\phi_1^i + \cdots, \tag{B 5}$$

represents the phase of the wave solution and therefore its spatial derivative $\boldsymbol{\nabla}_x\Theta$ corresponds to the local wavenumber. Now we consider the power series expansion of

$$\omega(\hat{\boldsymbol{x}},\hat{\boldsymbol{p}})\psi(\boldsymbol{x}) = \frac{1}{(2\pi\mu)^d}\iint \omega\left(\boldsymbol{x}+\frac{\boldsymbol{y}}{2},\boldsymbol{p}\right)\exp\left(\frac{-\mathrm{i}\boldsymbol{p}\cdot\boldsymbol{y}+\phi(\boldsymbol{x}+\boldsymbol{y})}{\mu}\right)\mathrm{d}\boldsymbol{y}\,\mathrm{d}\boldsymbol{p}, \tag{B 6}$$

where change of variable, $\boldsymbol{y}=\boldsymbol{x}'-\boldsymbol{x}$, is used in (2.8). We first derive

$$\begin{aligned}&\frac{1}{(2\pi\mu)^d}\iint \omega\left(\boldsymbol{x}+\frac{\boldsymbol{y}}{2},\boldsymbol{p}\right)\exp\left(\frac{-\mathrm{i}\boldsymbol{p}\cdot\boldsymbol{y}}{\mu}\right)\mathrm{d}\boldsymbol{y}\,\mathrm{d}\boldsymbol{p}\\ &\quad= \frac{1}{(2\pi\mu)^d}\iint\left(\omega(\boldsymbol{x},\boldsymbol{p})+\frac{1}{2}\boldsymbol{\nabla}_x\omega(\boldsymbol{x},\boldsymbol{p})\cdot\boldsymbol{y}+O(|\boldsymbol{y}|^2)\right)\exp\left(\frac{-\mathrm{i}\boldsymbol{p}\cdot\boldsymbol{y}}{\mu}\right)\mathrm{d}\boldsymbol{y}\,\mathrm{d}\boldsymbol{p}\\ &\quad= \frac{1}{(2\pi\mu)^d}\iint\left(\omega(\boldsymbol{x},\boldsymbol{p})+\frac{\mathrm{i}\mu}{2}\boldsymbol{\nabla}_x\omega(\boldsymbol{x},\boldsymbol{p})\cdot\boldsymbol{\nabla}_p+O(\mu^2)\right)\exp\left(\frac{-\mathrm{i}\boldsymbol{p}\cdot\boldsymbol{y}}{\mu}\right)\mathrm{d}\boldsymbol{y}\,\mathrm{d}\boldsymbol{p}\\ &\quad= \frac{1}{(2\pi\mu)^d}\iint\left(\omega(\boldsymbol{x},\boldsymbol{p})-\frac{\mathrm{i}\mu}{2}\boldsymbol{\nabla}_x\cdot\boldsymbol{\nabla}_p\omega(\boldsymbol{x},\boldsymbol{p})+O(\mu^2)\right)\\ &\qquad\times\exp\left(\frac{-\mathrm{i}\boldsymbol{p}\cdot\boldsymbol{y}}{\mu}\right)\mathrm{d}\boldsymbol{y}\,\mathrm{d}\boldsymbol{p}+(\mathrm{surf})\\ &\quad= \frac{1}{(2\pi\mu)^d}\iint\left(\omega_0(\boldsymbol{x},\boldsymbol{p})+\mu\left(\omega_1(\boldsymbol{x},\boldsymbol{p})-\frac{\mathrm{i}}{2}\boldsymbol{\nabla}_x\cdot\boldsymbol{\nabla}_p\omega_0(\boldsymbol{x},\boldsymbol{p})\right)+O(\mu^2)\right)\\ &\qquad\times\exp\left(\frac{-\mathrm{i}\boldsymbol{p}\cdot\boldsymbol{y}}{\mu}\right)\mathrm{d}\boldsymbol{y}\,\mathrm{d}\boldsymbol{p}+(\mathrm{surf}).\end{aligned} \tag{B 7}$$

Here the (surf) terms represent the contribution from the integral surface $|\boldsymbol{p}|=\infty$. By assuming that $\tilde{\psi}$ is sufficiently smooth, we may neglect these terms hereafter. Additionally using

$$\phi(\boldsymbol{x}+\boldsymbol{y}) = \phi(\boldsymbol{x})+\boldsymbol{\nabla}_x\phi(\boldsymbol{x})\cdot\boldsymbol{y}+\tfrac{1}{2}(\boldsymbol{\nabla}_x\otimes\boldsymbol{\nabla}_x)\phi(\boldsymbol{x})\cdot(\boldsymbol{y}\otimes\boldsymbol{y})+O(|\boldsymbol{y}|^3), \tag{B 8}$$

where $\otimes$ denotes the outer product, we derive from (B 2) the following expression:

$$\begin{aligned}&\sigma-\frac{1}{(2\pi\mu)^d}\iint\left[\exp\left(\frac{-\mathrm{i}(\boldsymbol{p}-\boldsymbol{\nabla}_x\phi_0(\boldsymbol{x}))\cdot\boldsymbol{y}}{\mu}\right)\right.\\ &\quad\left.\times\exp\left(-\mathrm{i}\mu\boldsymbol{\nabla}_x\phi_1^r(\boldsymbol{x})\cdot\boldsymbol{\nabla}_p+\mu\boldsymbol{\nabla}_x\phi_1^i(\boldsymbol{x})\cdot\boldsymbol{\nabla}_p-\frac{\mathrm{i}\mu}{2}(\boldsymbol{\nabla}_x\otimes\boldsymbol{\nabla}_x)\phi_0(\boldsymbol{x})\cdot(\boldsymbol{\nabla}_p\otimes\boldsymbol{\nabla}_p)\right)\right.\end{aligned}$$

https://doi.org/10.1017/jfm.2019.825 Published online by Cambridge University Press

$$\times \left(\omega_0(\boldsymbol{x},\boldsymbol{p}) + \mu \left(\omega_1(\boldsymbol{x},\boldsymbol{p}) - \frac{\mathrm{i}}{2}\nabla_x \cdot \nabla_p \omega_0(\boldsymbol{x},\boldsymbol{p}) \right) \right) \Bigg] \, \mathrm{d}\boldsymbol{y}\, \mathrm{d}\boldsymbol{p} = O(\mu^2), \tag{B 9}$$

which, after performing an integration, becomes

$$\sigma - \left[\exp\left(-\mathrm{i}\mu \nabla_x \phi_1^r(\boldsymbol{x}) \cdot \nabla_p + \mu \nabla_x \phi_1^i(\boldsymbol{x}) \cdot \nabla_p - \frac{\mathrm{i}\mu}{2} (\nabla_x \otimes \nabla_x)\phi_0(\boldsymbol{x}) \cdot (\nabla_p \otimes \nabla_p) \right) \right.$$
$$\left. \times \left(\omega_0(\boldsymbol{x},\boldsymbol{p}) + \mu \left(\omega_1(\boldsymbol{x},\boldsymbol{p}) - \frac{\mathrm{i}}{2}\nabla_x \cdot \nabla_p \omega_0(\boldsymbol{x},\boldsymbol{p}) \right) \right) \right]_{\boldsymbol{p}=\nabla_x\phi_0} = O(\mu^2). \tag{B 10}$$

Further expanding the exponential function, we obtain the leading- and first-order terms as

$$\sigma_0 = \omega_0(\boldsymbol{x},\boldsymbol{p}), \tag{B 11a}$$

$$\begin{aligned} \sigma_1 \;=\; & \omega_1(\boldsymbol{x},\boldsymbol{p}) - \frac{\mathrm{i}}{2}\nabla_x \cdot \nabla_p \omega_0(\boldsymbol{x},\boldsymbol{p}) - \mathrm{i}\nabla_x \phi_1^r(\boldsymbol{x}) \cdot \nabla_p \omega_0(\boldsymbol{x},\boldsymbol{p}) + \nabla_x \phi_1^i(\boldsymbol{x}) \cdot \nabla_p \omega_0(\boldsymbol{x},\boldsymbol{p}) \\ & - \frac{\mathrm{i}}{2}(\nabla_x \otimes \nabla_x)\phi_0(\boldsymbol{x}) \cdot (\nabla_p \otimes \nabla_p)\omega_0(\boldsymbol{x},\boldsymbol{p}), \end{aligned} \tag{B 11b}$$

where it should be reminded that the wavenumber is now evaluated at $\boldsymbol{p} = \nabla_x \phi_0(\boldsymbol{x})$. The real part of (B 11$b$) is

$$\sigma_1 = \omega_1(\boldsymbol{x},\boldsymbol{p}) + \nabla_x \phi_1^i \cdot \nabla_p \omega_0(\boldsymbol{x},\boldsymbol{p}), \tag{B 12}$$

which combined with (B 11a) yields

$$\sigma = \omega(\boldsymbol{x},\, \nabla_x(\phi_0(\boldsymbol{x}) + \mu\phi_1^i(\boldsymbol{x}))) + O(\mu^2). \tag{B 13}$$

From this expression, we understand that by redefining the local wavenumber as $\boldsymbol{p} = \nabla_x \Theta$, the dispersion relation $\sigma = \omega(\boldsymbol{x},\boldsymbol{p})$ is valid up to the first-order perturbation terms. Therefore, the symbol $\omega(\boldsymbol{x},\boldsymbol{p})$ derived by the present diagonalisation method yields a dispersion relation of at least first-order accuracy.

In addition, using the imaginary part of (B 11b) that is

$$\begin{aligned} 0 \;=\; & -\tfrac{1}{2}\nabla_x \cdot \nabla_p \omega_0(\boldsymbol{x},\boldsymbol{p}) - \nabla_x \phi_1^r(\boldsymbol{x}) \cdot \nabla_p \omega_0(\boldsymbol{x},\boldsymbol{p}) \\ & - \tfrac{1}{2}(\nabla_x \otimes \nabla_x)\phi_0(\boldsymbol{x}) \cdot (\nabla_p \otimes \nabla_p)\omega_0(\boldsymbol{x},\boldsymbol{p}), \end{aligned} \tag{B 14}$$

and defining the squared wave amplitude $E(\boldsymbol{x}) \equiv |\tilde{\psi}|^2$, we can derive the leading-order expression of an elementary conservation law for a steady wave train,

$$\nabla_x \cdot (\nabla_p \omega(\boldsymbol{x}, \boldsymbol{p}(\boldsymbol{x}))E(\boldsymbol{x})) = O(\mu). \tag{B 15}$$

Appendix C. Forced–dissipative system

In a general non-conservative system, linear wave motions are governed by an equation in the form of

$$\mathrm{i}\frac{\partial \boldsymbol{\psi}}{\partial t} = \hat{\boldsymbol{L}}\boldsymbol{\psi} + \boldsymbol{\gamma}, \tag{C 1}$$

https://doi.org/10.1017/jfm.2019.825 Published online by Cambridge University Press

where the operator $\hat{\boldsymbol{L}}$ is not necessarily Hermitian and $\boldsymbol{\gamma}$ represents external forcing. Supposing that $\hat{\boldsymbol{L}}$ can be diagonalised as $\hat{\boldsymbol{M}}\hat{\boldsymbol{L}}\hat{\boldsymbol{M}}^{-1} = \hat{\boldsymbol{\Omega}}$, transforming the state vector into $\boldsymbol{\psi}' = \hat{\boldsymbol{M}}\boldsymbol{\psi}$, the equation for the Wigner distribution function of the ith mode, $w(\boldsymbol{x}, \boldsymbol{p}) = \int \psi_i'(\boldsymbol{x} + \boldsymbol{x}'/2)\psi_i'^{\dagger}(\boldsymbol{x} - \boldsymbol{x}'/2)\mathrm{e}^{-\mathrm{i}\boldsymbol{p}\cdot\boldsymbol{x}'/\mu}\,\mathrm{d}\boldsymbol{x}'$, is derived,

$$\mathrm{i}\frac{\partial w}{\partial t} = \omega \star w - w \star \omega^{\dagger} + \mathrm{i}s, \tag{C 2}$$

where the source term is originates from $\boldsymbol{\gamma}$. The dispersion relation $\omega(\boldsymbol{x}, \boldsymbol{p})$ now has real and imaginary parts. Defining $\sigma = \mathrm{Re}\omega$ and $\nu = -2\mathrm{Im}\omega$, we may rewrite (C 2) as

$$\frac{\partial w}{\partial t} + \mu\nabla_p\sigma \cdot \nabla_x w - \mu\nabla_x\sigma \cdot \nabla_p w = -\nu w + s + O(\mu^2). \tag{C 3}$$

In a dissipative system, the function $\nu(\boldsymbol{x}, \boldsymbol{p})$ usually (but not necessarily) takes a positive value, representing the decay rate of wave energy. Equation (C 3) is also a kind of transport equation (1.2).

REFERENCES

AIKI, H., GREATBATCH, R. J. & CLAUS, M. 2017 Towards a seamlessly diagnosable expression for the energy flux associated with both equatorial and mid-latitude waves. *Prog. Earth Planet. Sci.* **4** (1), 11.

BENDER, C. M. & ORSZAG, S. A. 1999 *Advanced Mathematical Methods for Scientists and Engineers I: Asymptotic Methods and Perturbation Theory*. Springer.

BRETHERTON, F. P. 1968 Propagation in slowly varying waveguides. *Proc. R. Soc. Lond.* A **302** (1471), 555–576.

BÜHLER, O. 2014 *Waves and Mean Flows*, 2nd edn. Cambridge University Press.

BÜHLER, O., CALLIES, J. & FERRARI, R. 2014 Wave-vortex decomposition of one-dimensional ship-track data. *J. Fluid Mech.* **756**, 1007–1026.

BÜHLER, O., KUANG, M. & TABAK, E. G. 2017 Anisotropic Helmholtz and wave-vortex decomposition of one-dimensional spectra. *J. Fluid Mech.* **815**, 361–387.

CHASSANDE-MOTTIN, E. & PAI, A. 2005 Discrete time and frequency Wigner–Ville distribution: Moyal's formula and aliasing. *IEEE Signal Process. Lett.* **12**, 508–511.

CHOUKSEY, M., EDEN, C. & BRÜGGEMANN, N. 2018 Internal gravity wave emission in different dynamical regimes. *J. Phys. Oceanogr.* **48** (8), 1709–1730.

COHEN, L. 2012 *The Weyl Operator and its Generalization*. Springer Basel.

DANIOUX, E. & VANNESTE, J. 2016 Near-inertial-wave scattering by random flows. *Phys. Rev. Fluids* **1** (3), 033701.

EDEN, C. & OLBERS, D. 2017 A closure for eddy-mean flow effects based on the Rossby wave energy equation. *Ocean Model.* **114**, 59–71.

GÉRARD, P., MARKOWICH, P. A., MAUSER, N. J. & POUPAUD, F. 1997 Homogenization limits and Wigner transforms. *Commun. Pure Appl. Maths* **50** (4), 323–379.

GUO, M. & WANG, X. 1999 Transport equations for a general class of evolution equations with random perturbations. *J. Math. Phys.* **40** (10), 4828–4858.

HAIDVOGEL, D. B. & BECKMANN, A. 1999 *Numerical Ocean Circulation Modeling*. World Scientific.

KAFIABAD, H. A., SAVVA, M. A. C. & VANNESTE, J. 2019 Diffusion of inertia-gravity waves by geostrophic turbulence. *J. Fluid Mech.* **869**, R7.

KINOSHITA, T. & SATO, K. 2013 A formulation of unified three-dimensional wave activity flux of inertia-gravity waves and Rossby waves. *J. Atmos. Sci.* **70** (6), 1603–1615.

KINOSHITA, T., TOMIKAWA, Y. & SATO, K. 2010 On the three-dimensional residual mean circulation and wave activity flux of the primitive equations. *J. Met. Soc. Japan* **88** (3), 373–394.

https://doi.org/10.1017/jfm.2019.825 Published online by Cambridge University Press

KUBO, R. 1964 Wigner representation of quantum operators and its applications to electrons in a magnetic field. *J. Phys. Soc. Japan* **19** (11), 2127–2139.

KUNZE, E. 1985 Near-inertial wave propagation in geostrophic shear. *J. Phys. Oceanogr.* **15** (5), 544–565.

LIEN, R.-C. & MÜLLER, P. 1992 Normal-mode decomposition of small-scale oceanic motions. *J. Phys. Oceanogr.* **22** (12), 1583–1595.

LIGHTHILL, J. 1978 *Waves in Fluids*. Cambridge University Press.

LITTLEJOHN, R. G. & FLYNN, W. G. 1991 Geometric phases in the asymptotic theory of coupled wave equations. *Phys. Rev.* A **44** (8), 5239–5256.

MACHENHAUER, B. 1977 On the dynamics of gravity oscillations in a shallow water model, with applications to normal mode initialization. *Beitr. Phys. Atmos.* **50**, 253–271.

MACKINNON, J. A., ZHAO, Z., WHALEN, C. B., WATERHOUSE, A. F., TROSSMAN, D. S., SUN, O. M., LAURENT, L. C. S., SIMMONS, H. L., POLZIN, K., PINKEL, R. *et al.* 2017 Climate process team on internal wave-driven ocean mixing. *Bull. Am. Meteorol. Soc.* **98** (11), 2429–2454.

MATSUNO, T. 1966 Quasi-geostrophic motions in the equatorial area. *J. Met. Soc. Japan. Ser. II* **44** (1), 25–43.

MCDONALD, S. W. 1988 Phase-space representations of wave equations with applications to the eikonal approximation for short-wavelength waves. *Phys. Rep.* **158** (6), 337–416.

MCKEE, W. D. 1973 Internal-inertia waves in a fluid of variable depth. *Math. Proc. Camb. Phil. Soc.* **73** (1), 205–213.

MORRISON, P. J. 1998 Hamiltonian description of the ideal fluid. *Rev. Mod. Phys.* **70** (2), 467–521.

OLBERS, D. & EDEN, C. 2013 A global model for the diapycnal diffusivity induced by internal gravity waves. *J. Phys. Oceanogr.* **43** (8), 1759–1779.

PEDLOSKY, J. 1987 *Geophysical Fluid Dynamics*. Springer.

PETRUCCIONE, F. & BREUER, H.-P. 2002 *The Theory of Open Quantum Systems*. Oxford University Press.

PLUMB, R. A. 1985 On the three-dimensional propagation of stationary waves. *J. Atmos. Sci.* **42** (3), 217–229.

POWELL, J. M. & VANNESTE, J. 2005 Transport equations for waves in randomly perturbed Hamiltonian systems, with application to Rossby waves. *Wave Motion* **42** (4), 289–308.

RYZHIK, L., PAPANICOLAOU, G. & KELLER, J. B. 1996 Transport equations for elastic and other waves in random media. *Wave Motion* **24** (4), 327–370.

SAKURAI, J. J. & NAPOLITANO, J. 2011 *Modern Quantum Mechanics*. Addison-Wesley.

SATO, K., KINOSHITA, T. & OKAMOTO, K. 2013 A new method to estimate three-dimensional residual-mean circulation in the middle atmosphere and its application to gravity wave-resolving general circulation model data. *J. Atmos. Sci.* **70** (12), 3756–3779.

SAVVA, M. A. C. & VANNESTE, J. 2018 Scattering of internal tides by barotropic quasigeostrophic flows. *J. Fluid Mech.* **856**, 504–530.

SHEPHERD, T. G. 1990 Symmetries, conservation laws, and Hamiltonian structure in geophysical fluid dynamics. *Adv. Geophys.* **32**, 287–338.

TAKAYA, K. & NAKAMURA, H. 1997 A formulation of a wave-activity flux for stationary Rossby waves on a zonally varying basic flow. *Geophys. Res. Lett.* **24**, 2985–2988.

TAKAYA, K. & NAKAMURA, H. 2001 A formulation of a phase-independent wave-activity flux for stationary and migratory quasigeostrophic eddies on a zonally varying basic flow. *J. Atmos. Sci.* **58** (6), 608–627.

VANNESTE, J. 2013 Balance and spontaneous wave generation in geophysical flows. *Annu. Rev. Fluid Mech.* **45**, 147–172.

VANNESTE, J. & SHEPHERD, T. G. 1999 On wave action and phase in the non–canonical Hamiltonian formulation. *Proc. R. Soc. Lond.* A **455**, 3–21.

WAMDI GROUP 1988 The WAM model – a third generation ocean wave prediction model. *J. Phys. Oceanogr.* **18** (12), 1775–1810.

WARN, T., BOKHOVE, O., SHEPHERD, T. G. & VALLIS, G. K. 1995 Rossby number expansions, slaving principles, and balance dynamics. *Q. J. R. Meteorol. Soc.* **121** (523), 723–739.

https://doi.org/10.1017/jfm.2019.825 Published online by Cambridge University Press

WHITHAM, G. B. 1970 Two-timing, variational principles and waves. *J. Fluid Mech.* **44** (2), 373–395.

WORDSWORTH, R. D. 2009 A phase-space study of jet formation in planetary-scale fluids. *Phys. Fluids* **21** (5), 056602.

YASUDA, Y., SATO, K. & SUGIMOTO, N. 2015 A theoretical study on the spontaneous radiation of inertia–gravity waves using the renormalization group method. Part I. Derivation of the renormalization group equations. *J. Atmos. Sci.* **72** (3), 957–983.

YIĞIT, E. & MEDVEDEV, A. S. 2015 Internal wave coupling processes in Earth's atmosphere. *Adv. Space Res.* **55** (4), 983–1003.

ŽAGAR, N., KASAHARA, A., TERASAKI, K., TRIBBIA, J. & TANAKA, H. 2015 Normal-mode function representation of global 3-D data sets: open-access software for the atmospheric research community. *Geosci. Model Develop.* **8**, 1169–1195.

https://doi.org/10.1017/jfm.2019.825 Published online by Cambridge University Press